

<sub>1</sub> Study of neutrino-nucleus interaction at around 1 GeV using  
<sub>2</sub> hollow cuboid lattice neutrino detectors, WAGASCI, muon  
<sub>3</sub> range detectors and magnetized spectrometer, Baby MIND,  
<sub>4</sub> at J-PARC neutrino monitor hall

<sub>5</sub> A. Bonnemaison, R. Cornat, L. Domine, O. Drapier, O. Ferreira, F. Gastaldi,  
<sub>6</sub> M. Gonin, J. Imber, M. Licciardi, F. Magniette, T. Mueller, L. Vignoli, and O. Volcy

<sub>7</sub> *Ecole Polytechnique, IN2P3-CNRS, Laboratoire Leprince-Ringuet, Palaiseau,*  
<sub>8</sub> *France*

<sub>9</sub> S. Cao and T. Kobayashi

<sub>10</sub> *High Energy Accelerator Research Organization (KEK), Tsukuba, Ibaraki, Japan*

<sub>11</sub> M. Khabibullin, A. Khotjantsev, A. Kostin, Y. Kudenko, A. Mefodiev, O. Mineev,  
<sub>12</sub> S. Suvorov, and N. Yershov

<sub>13</sub> *Institute for Nuclear Research of the Russian Academy of Sciences, Moscow, Russia*

<sub>14</sub> B. Quilain

<sub>15</sub> *Kavli Institute for the Physics and Mathematics of the Universe (WPI), The*  
<sub>16</sub> *University of Tokyo Institutes for Advanced Study, University of Tokyo, Kashiwa,*  
<sub>17</sub> *Chiba, Japan*

<sub>18</sub> T. Hayashino, A. Hiramoto, A.K. Ichikawa, K. Nakamura, T. Nakaya, K Yasutome,  
<sub>19</sub> and K. Yoshida

<sub>20</sub> *Kyoto University, Department of Physics, Kyoto, Japan*

<sub>21</sub> Y. Azuma, J. Harada, T. Inoue, K. Kin, N. Kukita, S. Tanaka, Y. Seiya,  
<sub>22</sub> K. Wakamatsu, and K. Yamamoto

<sub>23</sub> *Osaka City University, Department of Physics, Osaka, Japan*

<sup>24</sup> A. Blondel, F. Cadoux, Y. Favere, E. Noah, L. Nicola, and S. Parsa

<sup>25</sup> *University of Geneva, Section de Physique, DPNC, Geneva, Switzerland*

<sup>26</sup> N. Chikuma, F. Hosomi, T. Koga, R. Tamura, and M. Yokoyama

<sup>27</sup> *University of Tokyo, Department of Physics, Tokyo, Japan*

<sup>28</sup> Y. Hayato

<sup>29</sup> *University of Tokyo, Institute for Cosmic Ray Research, Kamioka Observatory,  
30 Kamioka, Japan*

<sup>31</sup> Y. Asada, K. Matsushita, A. Minamino, K. Okamoto, and D. Yamaguchi

<sup>32</sup> *Yokohama National University, Faculty of Engineering, Yokohama, Japan*

<sup>33</sup> December 14, 2017

# **34** Contents

|           |          |  |           |
|-----------|----------|--|-----------|
| <b>35</b> | <b>1</b> | <b>Introduction</b>  | <b>4</b>  |
| <b>36</b> | <b>2</b> | <b>Experimental Setup</b>  | <b>5</b>  |
| 37        | 2.1      | WAGASCI modules . . . . .  | 6         |
| 38        | 2.1.1    | Detector . . . . .   | 6         |
| 39        | 2.1.2    | Electronics . . . . .  | 9         |
| 40        | 2.1.3    | Water system . . . . .   | 10        |
| 41        | 2.2      | INGRID Proton module . . . . .   | 10        |
| 42        | 2.3      | Baby MIND . . . . .  | 12        |
| 43        | 2.3.1    | Magnet modules . . . . .   | 12        |
| 44        | 2.3.2    | Scintillator modules . . . . .   | 13        |
| 45        | 2.3.3    | Electronics . . . . .  | 15        |
| 46        | 2.3.4    | Pefromance check . . . . .   | 16        |
| 47        | 2.4      | Side muon range detector . . . . .                                     | 17        |
| <b>48</b> | <b>3</b> | <b>Physics goals</b>   | <b>19</b> |
| 49        | 3.1      | Expected number of events . . . . .                                    | 20        |
| 50        | 3.2      | Pseudo-monochromatic beam by using different off-axis fluxes . . . . . | 20        |
| 51        | 3.3      | Extraction of Cross sections . . . . .                                 | 20        |
| 52        | 3.4      | Subjects WAGASCI can contribute . . . . .                              | 22        |
| <b>53</b> | <b>4</b> | <b>Status of J-PARC T59 experiment</b>                                 | <b>24</b> |
| <b>54</b> | <b>5</b> | <b>MC studies</b>  | <b>27</b> |
| 55        | 5.1      | Simulation setup . . . . .   | 27        |
| 56        | 5.2      | Event selection . . . . .  | 27        |
| <b>57</b> | <b>6</b> | <b>Standalone WAGASCI-module performances</b>                          | <b>30</b> |
| 58        | 6.1      | Reconstruction algorithm . . . . .                                     | 32        |
| 59        | 6.1.1    | Description . . . . .  | 32        |
| 60        | 6.1.2    | Performances . . . . .   | 34        |
| 61        | 6.2      | Background substraction: the water-out module . . . . .                | 38        |
| <b>62</b> | <b>7</b> | <b>Schedule</b>  | <b>41</b> |
| <b>63</b> | <b>8</b> | <b>Requests</b>  | <b>41</b> |
| 64        | 8.1      | Neutrino beam . . . . .  | 41        |
| 65        | 8.2      | Equipment request including power line . . . . .                       | 41        |

## Abstract

67 We propose to study the neutrino-nucleus interaction around 1 GeV at the B2 floor  
 68 of the T2K neutrino monitor building. Our experimental setup contains two hollow  
 69 cuboid lattice detectors as the neutrino interaction target (known as WAGASCI  
 70 modules), two side- and one downstream- muon range detectors(MRD's). The downstream-  
 71 MRD, so called the Baby MIND detector, also works as a magnet and provides the  
 72 charge identification capability. Most of the detectors have already been constructed  
 73 and have been commissioned in the J-PARC T59 experiment and the CERN neutrino  
 74 platform. Therefore, the collaboration will be ready to proceed to the physics data  
 75 taking for the T2K beam time in January 2019.

76 We will provide the differential cross sections of the charged current neutrino and  
 77 antineutrino interactions on water and hydrocarbon with slightly higher neutrino en-  
 78 ergy than T2K ND280 with wide angler acceptance. In addition, by combining our  
 79 measurements with those from ND280, model-independent extraction of the cross sec-  
 80 tion for narrow energy spread becomes possible. These measurements would greatly  
 81 improve the understanding of the neutrino interaction at around 1 GeV and contribute  
 82 to reducing one of the most significant uncertainties of the T2K experiment.

## 83 1 Introduction

84 The understanding of neutrino-nucleus interactions in the 1 GeV energy region is critical  
 85 for the success of accelerator-based neutrino oscillation experiments such as the T2K exper-  
 86 iment. Complicated multi-body effects of nuclei render this understanding difficult. The  
 87 T2K near detectors have been measuring these and significant progress has been achieved.  
 88 However, the understanding is still limited. One of the big factors preventing a complete  
 89 understanding is the non-monochromatic neutrino beam spectrum. Measurements with  
 90 distinct but partially overlapping beam spectra would be a great benefit in resolving the  
 91 contribution from different neutrino energies. We, the WAGASCI collaboration, proposes  
 92 to study the neutrino-nucleus interaction at the B2 floor of the neutrino monitor building,  
 93 where different neutrino spectra from the T2K off-axis near detector (ND280) can be ob-  
 94 tained due to the different off-axis position. Our experimental setup contains two hollow  
 95 cuboid lattice detectors as the neutrino interaction target (known as WAGASCI modules),  
 96 two side- and one downstream- muon range detectors(MRD's). We will have two types of  
 97 the WAGASCI modules, a water-in module and a water-out module. The water-in WA-  
 98 GASCI module has water the hollow cuboid lattice, and the water-out WAGASCI module  
 99 doesn't have water inside the lattice. The hollow cuboid lattice and side-MRD's allow a  
 100 measurement of wider-angle scattering than ND280. High water to scintillator material  
 101 ratio enables the measurement of the neutrino interaction with water, which is highly de-  
 102 sired for the T2K experiment because it's far detector, Super-Kamiokande, is composed of  
 103 water. The MRD's consist of plastic scintillators and iron plates. The downstream-MRD,  
 104 so called the Baby MIND detector, also works as a magnet and provides the charge iden-  
 105 tification capability as well as magnetic momentum measurement for high energy muons.

106 The charge identification is essentially important to select antineutrino events in the an-  
107 tineutrino beam because contamination of the neutrino events is as high as 30%. Most of  
108 the detectors have already been constructed. The WAGASCI modules have been commis-  
109 sioned as the J-PARC T59 experiment and the Baby MIND detector was commissioned at  
110 the CERN neutrino platform. Therefore, the collaboration will be ready to proceed to the  
111 physics data taking for the T2K beam time in January 2019. We will provide the cross sec-  
112 tions of the charged current neutrino and antineutrino interactions on water with slightly  
113 higher neutrino energy than T2K ND280 with wide angler acceptance. When combined  
114 with ND280 measurements, our measurement would greatly improve the understanding  
115 of the neutrino interaction at around 1 GeV and contribute to reducing one of the most  
116 significant uncertainties of the T2K experiment.

## 117 2 Experimental Setup

118 Figure 1 and 2 show a schematic view and a CAD drawing of the entire set of detectors.  
119 Central neutrino target detectors consist of two WAGASCI modules and T2K INGRID  
120 proton module. Inside the WAGASCI module, plastic scintillator bars are aligned as a  
121 hollow cuboid lattice and spaces in the lattice are filled with water for a water-in WAGASCI  
122 module. T2K INGRID proton module is a full active neutrino target detector which is  
123 composed only with scintillator bars in its tracking region. The central detectors are  
124 surrounded by two side- and one downstream- muon range detectors(MRD's) The MRD's  
125 are used to select muon tracks from the charged-current (CC) interactions and to reject  
126 short tracks caused by neutral particles that originate mainly from neutrino interactions in  
127 material surrounding the central detector, like the walls of the detector hall, neutrons and  
128 gammas, or neutral-current (NC) interactions. The muon momentum can be reconstructed  
129 from its range inside the detector. The MRD's consist of plastic scintillators and iron plates.  
130 The downstream-MRD, also known as the Baby MIND detector, additionally has a coil  
131 wound around each of the iron plates so it may be magnetized. This provides the charge  
132 selection capability.

133 For all detectors, scintillation light in the scintillator bar is collected and transported  
134 to a photodetector with a wavelength shifting fiber (WLS fiber). The light is read out by  
135 a photodetector, Multi-Pixel Photon Counter (MPPC), attached to one end of the WLS  
136 fiber. The signal from the MPPC is read out by the dedicated electronics developed for  
137 the test experiment to enable bunch separation in the beam spill. The readout electronics  
138 are triggered using the beam-timing signal from MR to synchronize to the beam. The  
139 beam-timing signal is branched from those for T2K, and will not effect T2K data taking.

140 T2K adopted the off-axis beam method, in which the neutrino beam is intentionally  
141 directed 2.5 degrees away from SK producing a narrow band  $\nu_\mu$  beam. The off-axis near  
142 detector, ND280, is installed towards the SK direction in the B1 floor of the near detector  
143 hall of the J-PARC neutrino beam-line. We propose to install our detector in the B2 floor

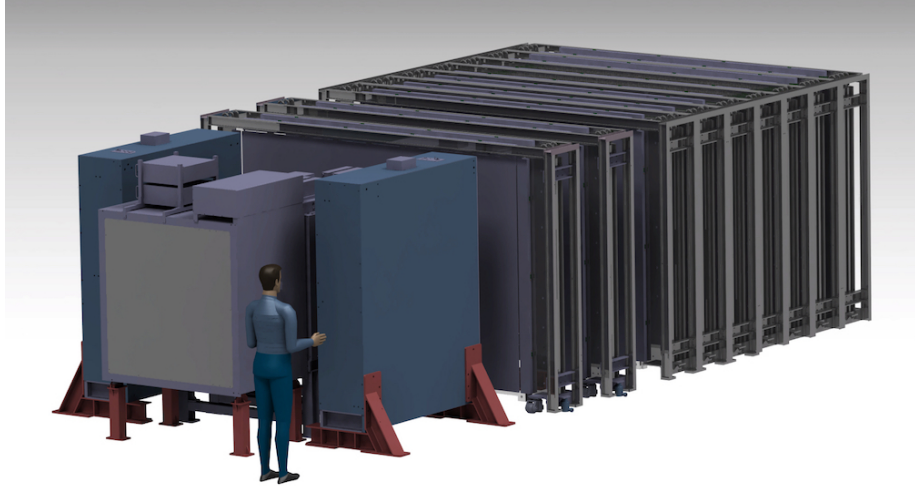


Figure 1: Schematic view of entire sets of detectors.

<sup>144</sup> of the near detector hall, where the off-axis angle of 1.5 degrees is slightly different to the  
<sup>145</sup> 2.5 degrees of ND280. The candidate detector position in the B2 floor is shown in Figure  
<sup>146</sup> 3. The expected neutrino energy spectrum at the candidate position is shown in Figure 4.

## <sup>147</sup> 2.1 WAGASCI modules

### <sup>148</sup> 2.1.1 Detector

<sup>149</sup> The WAGASCI modules are mainly composed of 1280 plastic scintillator bars and a sur-  
<sup>150</sup> rounding stainless steel tank as shown in Figure 5. The total number of channels in one  
<sup>151</sup> WAGASCI module is 1280. The stainless steel tank is constructed by welding stainless  
<sup>152</sup> steel plates, is sized as 460mm×1250mm×1250 mm, and weighs 0.5 tonne.

<sup>153</sup> One WAGASCI module consists of 16 scintillator tracking planes, where each plane  
<sup>154</sup> is an array of 80 scintillator bars fixed with ABS frames. The 40 bars, called parallel  
<sup>155</sup> scintillators, are placed perpendicularly to the beam, and the other 40 bars, called lattice  
<sup>156</sup> scintillators, are placed in parallel to the beam with hollow cuboid lattice in the tracking  
<sup>157</sup> plane as shown in Figure 5. Thanks to the hollow cuboid lattice of the scintillator bars,  
<sup>158</sup> the WAGASCI module has  $4\pi$  angular acceptance for charged particles.

<sup>159</sup> Thin plastic scintillator bars produced at Fermilab by extrusion method, mainly consists  
<sup>160</sup> of polystyrene and are surrounded by thin reflector including  $\text{TiO}_2$  (3 mm in thickness)  
<sup>161</sup> are used for the WAGASCI modules to reduce the mass ratio of scintillator bars to water,  
<sup>162</sup> because neutrino interactions in the scintillator bars are a background for the cross section  
<sup>163</sup> measurements on  $\text{H}_2\text{O}$ . Each scintillator bar is sized as 1020mm×25mm×3 mm including

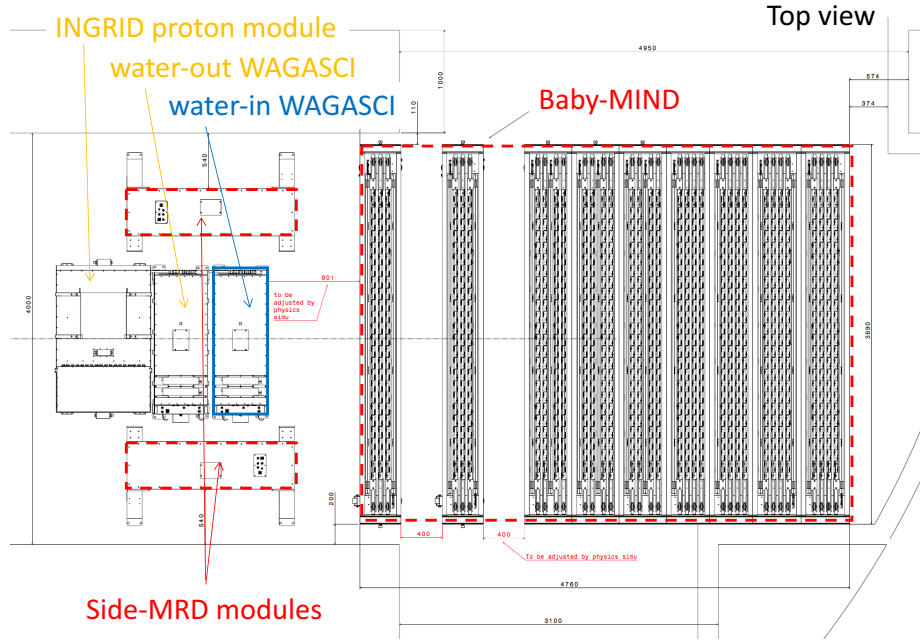


Figure 2: Top view of entire sets of detectors.

164 the reflector part, and half of all the scintillator bars have 50-mm-interval slits to form the  
 165 hollow cuboid lattice (Figure 6 ).

166 We will have two types of the WAGASCI modules, a water-in module and a water-out  
 167 module. The water-in WAGASCI module has water in spaces of the hollow cuboid lattice.  
 168 The total water mass serving as neutrino targets in the fiducial volume of the module is  
 169 188 kg, and the mass ratio of scintillator bars to water is 80 %. The water-out WAGASCI  
 170 module doesn't have water inside the detector. The total CH mass serving as neutrino  
 171 target in the fiducial volume of the module is 47 kg, and the mass fraction of scintillator  
 172 bars is 100 %.

173 Scintillation light is collected by wave length shifting fibers, Y-11 (non-S type with a  
 174 diameter of 1.0 mm produced by Kuraray. A fiber is glued by optical cement in a groove  
 175 on surface of a scintillator bar. 32 fibers are gathered together by a fiber bundle at edge  
 176 of the module, and lead scintillation light to a 32-channel arrayed MPPC. Since crosstalk  
 177 of light yield due to reflection on the inner surface of each cell has been observed, all the  
 178 scintillator bars are painted black by aqueous color spray. It is confirmed by measurements  
 179 with cosmic rays that black painting on the surface of the scintillator bars suppresses this  
 180 crosstalk so that no significant crosstalk effect is observed within uncertainty.

181 32-channel arrayed MPPCs, as shown in the Figure 7, are used for the modules. The

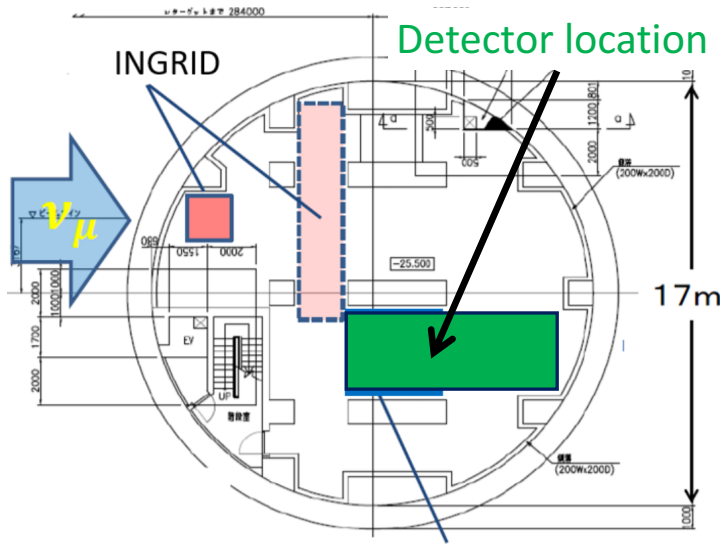


Figure 3: Candidate detector position on the B2 floor of the near detector hall.

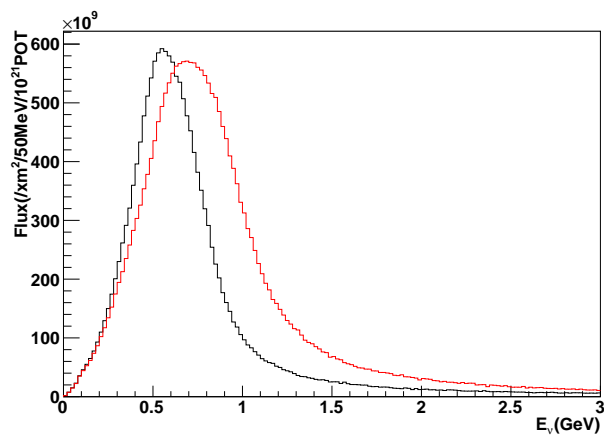


Figure 4: Neutrino energy spectrum at the candidate detector position (red, off-axis 1.5 degree). The spectrum at the ND280 site (black, off-axis 2.5 degree) is also shown.

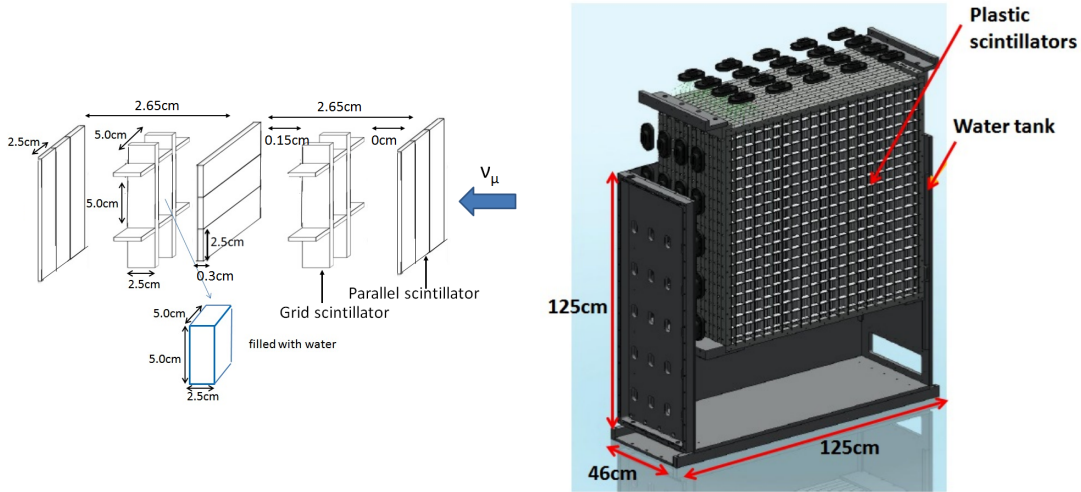


Figure 5: Schematic views of hollow cuboid lattice of plastic scintillator bars (left) and WAGASCI module (right).

182 surface of the fiber bundle is polished and directly attached onto the 32-channel arrayed  
 183 MPPCs. The positions of 32 fibers on the bundle are aligned to fit the channels of MPPCs.  
 184 The MPPC is a product of Hamamatsu Photonics, S13660(ES1), with suppressed noise  
 185 rate of  $\sim 6$  kHz per channel at 0.5 p.e. threshold. For each MPPC channel, 716 pixels of  
 186 APD are aligned in a shape of circle.

187 **2.1.2 Electronics**

188 As front-end electronics of this detector, a Silicon PM Integrated Read-Out Chip (SPIROC)  
 189 [13] is adopted. SPIROC is a 36-channel auto-triggered front-end ASIC, and is produced  
 190 by OMEGA/ IN2P3. It not only contains an analog signal processing part such as amplifi-  
 191 cation and shaping of the waveform, but contains a digital signal processing parts such as  
 192 auto-trigger and timing measurement. Charge of MPPC signal is sampled by track-and-  
 193 hold circuit. A Front-end electronics board, Active Sensor Unit (ASU), has been developed  
 194 with the SPIROC2D chip, which is the latest version of SPIROC. Each readout board is  
 195 designed to control a 32-channel arrayed MPPC, and 40 of the ASU boards are aligned on  
 196 the module surface. The data acquisition system used for this detector, including back-end  
 197 boards, has been developed for prototypes of ultra-granular calorimeters for the Interna-  
 198 tional Linear Collider (ILC) [6], and independent of the T2K DAQ system. To synchronize  
 199 the DAQ system to J- PARC neutrino beam, pre-beam trigger and beam trigger are sent to  
 200 the clock control card. The beam trigger signals are converted from optical signals to NIM  
 201 signals at NIM module on the B2 floor. In addition, the information of spill number are

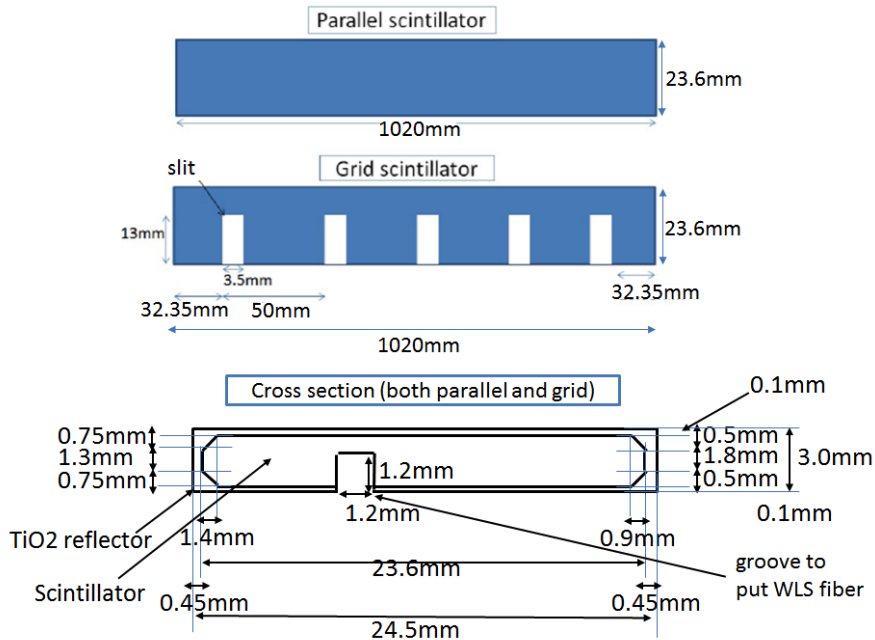


Figure 6: Geometry of scintillators used for WAGASCI modules.

202 delivered with 16-bit ECL level signals, and converted to an Ethernet frame by an FPGA  
 203 evaluation board to be directly sent to the DAQ PC. The electronics readout scheme is  
 204 shown in Figure 8.

205 **2.1.3 Water system**

206 Pure water is filled to the water tank of the water-in WAGASCI module as follows. First,  
 207 the water storage tank located at the B2 floor of the NM pit is filled with water delivered  
 208 from a water tap on the ground level through a long hose. Second, the water is pumped  
 209 to the other water storage tank though a water filler to produce pure water. Third, a  
 210 compound preservative called Germall plus, which is the same preservative used in one of  
 211 the sub-detectors of T2K ND280, FGD2, is put into the water to keep water from being  
 212 bad. Then, the water is poured to the water-in WAGASCI module, and it is kept in the  
 213 module during the neutrino beam operation and not to be circulated.

214 **2.2 INGRID Proton module**

215 INGRID Proton module is a neutrino detector of the T2K experiment. It is a fully-active  
 216 tracking detector which consists of only scintillator strips. The purpose of this Proton

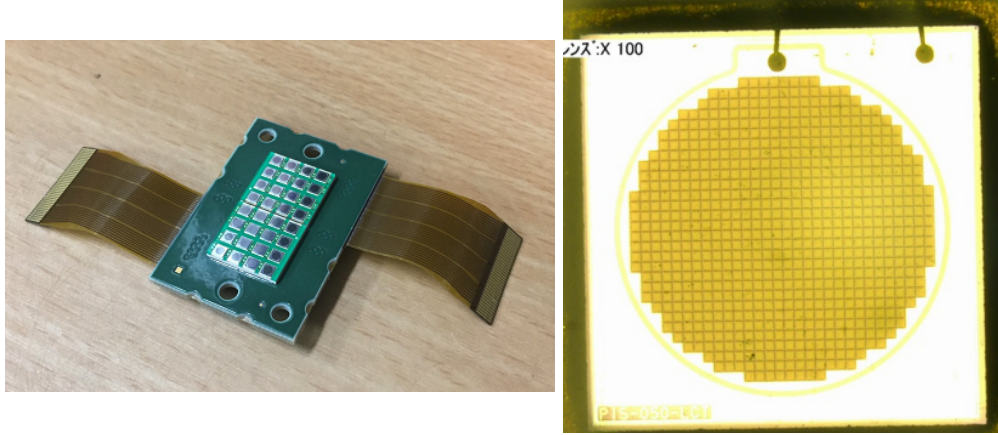


Figure 7: 32-channel arrayed MPPC (left) and an enlarged view of one MPPC channel (right).

217 Module is to separate the neutrino interaction types by detecting the protons and pions  
 218 together with the muons from the neutrino interactions, and to measure the neutrino cross  
 219 section for each interaction type. It consists of 36 tracking planes surrounded by veto  
 220 planes (Figure 9), where each tracking plane is an array of two types of scintillator strips.  
 221 The 16 strips in the inner region have dimensions of  $25\text{mm} \times 13\text{mm} \times 1200\text{mm}$ , while the 16  
 222 strips in the outer region have dimensions of  $50\text{mm} \times 10\text{mm} \times 1200\text{mm}$ , making a plane of  
 223  $1200\text{mm} \times 1200\text{mm}$  in the horizontal and vertical directions. The former is the scintillator  
 224 produced for the K2K SciBar detector [4] and the latter was produced for INGRID. The  
 225 tracking planes are placed perpendicular to the beam axis at 23mm intervals. Since the  
 226 strips are aligned in one direction, each tracking plane is sensitive to either the horizontal or  
 227 vertical position of the tracks. The tracking planes are therefore placed alternating in the  
 228 horizontal and vertical directions so that three-dimensional tracks can be reconstructed.  
 229 The tracking planes also serve as the neutrino interaction target. As with the WAGASCI  
 230 modules, scintillation light is read out by a WLS fiber and MPPC.

231 It was installed on the neutrino beam axis on the SS floor of the T2K near detector hall  
 232 in 2010, and had been used for neutrino cross section measurements. In August 2017, it  
 233 was moved to the B2 floor of the T2K near detector hall by J-PARC T59 after getting the  
 234 approval from T2K to use them. J-PARC T59 is performing a neutrino beam measurement  
 235 using the detector from October 2017, and the measurement will continue until May 2018  
 236 as we will discuss in Sec. 4.

237 We will operate the INGRID Proton module using the T2K near detector electronics/DAQ  
 238 system in the same way as J-PARC T59. A proposal to use the module and its  
 239 electronics for our project will be submitted to the T2K collaboration.

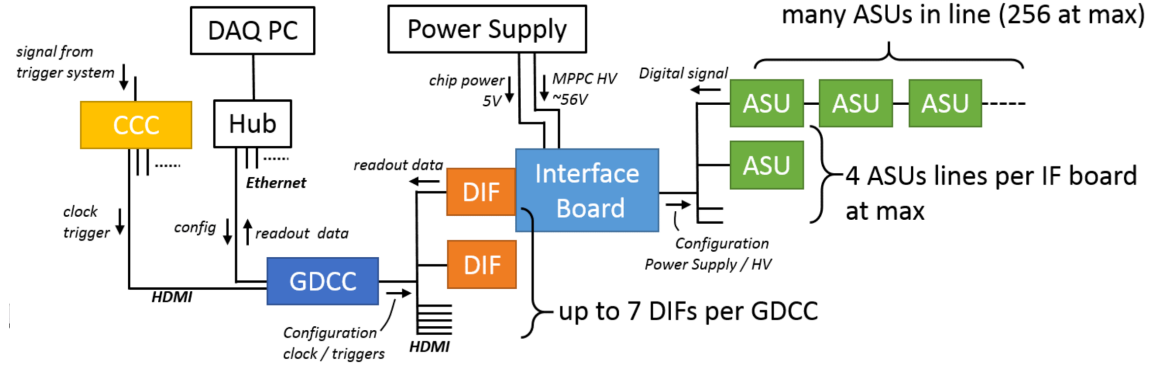


Figure 8: WAGASCI electronics readout scheme.

### 2.3 Baby MIND

The Baby MIND is the downstream Muon Range Detector. It also works as a magnet and provides the charge identification capability as well as magnetic momentum measurement for high energy muons.

The Baby MIND collaboration <sup>1</sup> submitted a proposal to the SPSC at CERN, SPSC-P-353. The project was approved by the CERN research board as Neutrino Platform project NP05 and constructed. The detector consists of 33 magnet modules, each 3500 mm × 2000 mm × 50 mm (30 mm steel) with a mass of approximately 2 tonnes. Of these magnet modules, 18 are instrumented with plastic scintillator modules.

#### 2.3.1 Magnet modules

Traditional layouts for magnetized iron neutrino detectors (e.g. MINOS) tend to be monolithic blocks with a unique pitch between consecutive steel segments and large conductor coils threaded around the whole magnet volume. The Baby MIND detector, like traditional designs, is built from sheets of iron interleaved with scintillator detector modules. However Baby MIND is novel in that the iron segments are all individually magnetized as shown in

---

<sup>1</sup>Contact person: E. Noah, Spokesperson: A. Blondel, Deputy spokesperson: Y. Kudenko

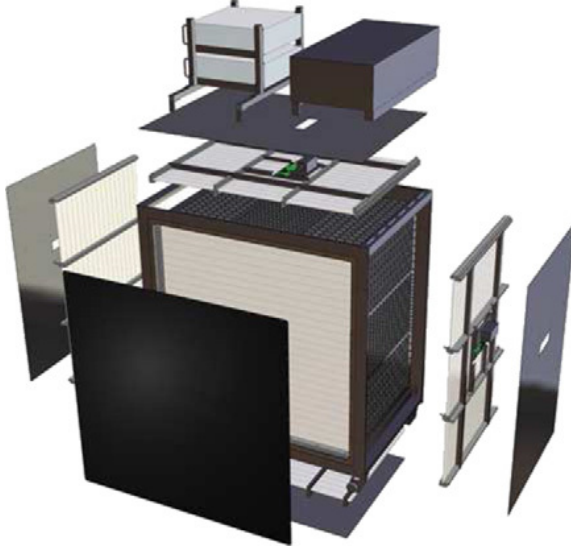


Figure 9: Schematic view of INGRID Proton module.

255 Figure 10, allowing for far greater flexibility in the setting of the pitch between segments,  
256 and in the allowable geometries that these detectors can take.

257 The key design outcome is a highly optimized magnetic field map. A double-slit config-  
258 uration for coil winding was adopted to increase the area over which the magnetic flux  
259 lines are homogeneous in  $B_x$  across the central tracking region. Simulations show the  
260 magnet field map to be very uniform over this central tracking region covering an area of  
261  $2800 \times 2000 \text{ mm}^2$ , Figure 11. The  $B_x$  component dominates in this region, with negligible  
262  $B_y$  and  $B_z$ . This was confirmed by measuring the field with 9 pick-up coils wound around  
263 the first module. Subsequent modules were equipped with one pick-up coil. Test results  
264 on the 33 modules show all achieve the required field of 1.5 T for a current of 140 A, with  
265 a total power consumption of 11.5 kW. The polarity of the field map shown in Figure 11  
266 (middle) can be reversed by changing the power supply configuration.

267 **2.3.2 Scintillator modules**

268 Each of the 18 scintillator modules is constructed from 2 planes of horizontal counters (95  
269 counters in total) and 2 planes of vertical counters (16 counters in total) [3], arranged  
270 with an overlap between planes to achieve close to 100% hit efficiency for minimum ioniz-  
271 ing muons. The arrangement of planes within a module is vertical-horizontal-horizontal-  
272 vertical. This arrangement was the result of an assembly approach whereby each plane  
273 was built from 2 half-planes, with each half plane consisting of a horizontal plane and a  
274 vertical plane. The scintillator bars are held in place using structural ladders that align

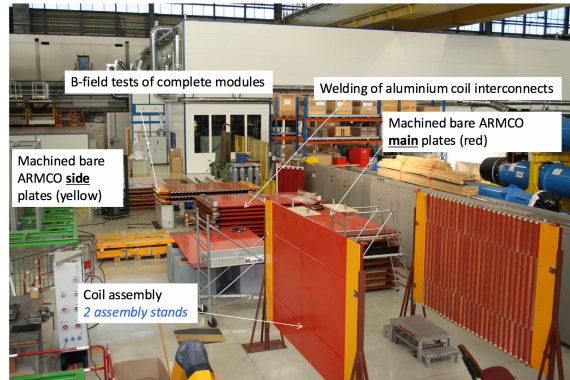


Figure 10: Magnet assembly zone at CERN.

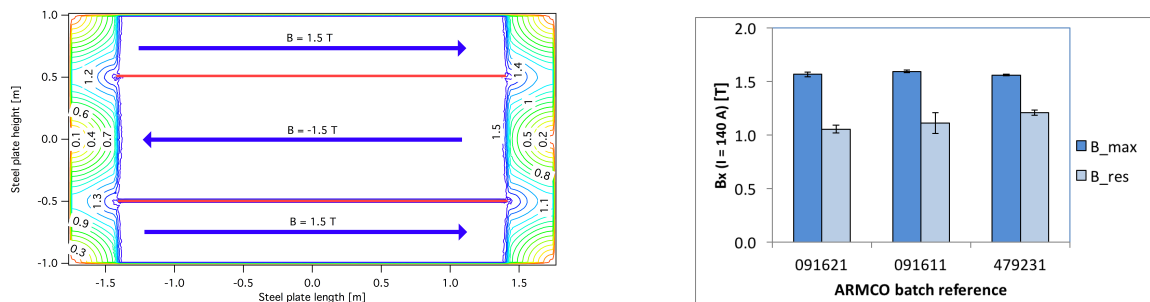


Figure 11: Left) Magnetic field map with a coil along 2800 mm of the length of the plate. Right) Measured B field for 33 modules.

275 and maintain the counters, Figure 12. No glue is used in the process, so counters can be  
276 replaced. Aluminum sheets front and back provide light tightness.



Figure 12: Scintillator modules assembly. Left) top of front half-module showing vertical counters, and the spacer-ladders that set the pitch between horizontal counters and hold them in place. Middle) rear half-module showing horizontal counters on their ladders. Right) Assembled rear half-module, the front half-module can be seen in the background.

277 The plastic scintillator counters were made from 220 mm-wide slabs, consisting of  
278 extruded polystyrene doped with 1.5% paraterphenyl (PTP) and 0.01% POPOP. They were  
279 cut to size then covered with a 30-100  $\mu\text{m}$  thick diffuse reflector resulting from etching of the  
280 surface with a chemical agent [10, 11]. The horizontal counter size is  $2880 \times 31 \times 7.5 \text{ mm}^3$ ,  
281 with one groove along the length of the bar in which sits a wavelength shifting fiber from  
282 Kuraray. The vertical counter size is  $1950 \times 210 \times 7.5 \text{ mm}^3$ , with one U-shaped groove  
283 along the bar. On each counter, two custom connectors house silicon photomultipliers,  
284 MPPC type S12571-025C from Hamamatsu, either side of the horizontal counter, and  
285 both connectors at the top for the vertical counter. This geometrical configuration for  
286 vertical counters was chosen for ease of connectivity to the electronics, and maintenance  
287 operations.

288 A total of 1744 horizontal counters and 315 vertical counters (including spares) were  
289 produced at the Uniplast company (Vladimir, Russia).

### 290 2.3.3 Electronics

291 The Baby MIND electronic readout scheme includes several custom-designed boards [12].  
292 The revised version is shown in Figure 13. At the heart of the system is the electronics  
293 Front End Board (FEB), developed by the University of Geneva. The readout system  
294 includes two ancillary boards, the Backplane, and the Master Clock Board (MCB) whose  
295 development has been managed by INRNE (Bulgarian Academy of Sciences) collaborators.

296 The FEBv2 hosts 3 CITIROC chips that can each read in signals from 32 SiPMs [7].  
297 Each signal input is processed by a high gain (HG), and a separate low gain (LG), signal  
298 path. The outputs from the slow shapers can be sampled using one of two modes: a  
299 mode with an externally applied delay, and a peak detector mode. A faster shaper can be  
300 switched to either HG or LG paths, followed by discriminators with adjustable thresholds

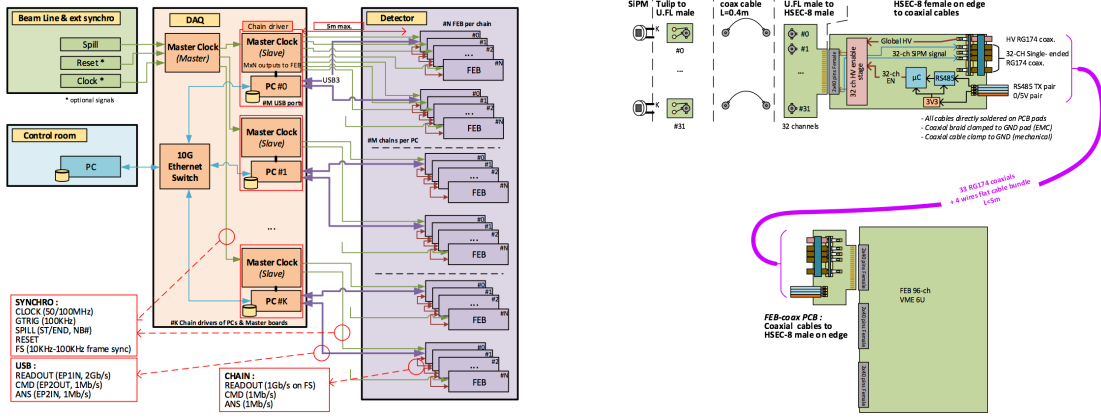


Figure 13: Left) Baby MIND electronics readout scheme. Right) SiPM-to-FEB connectivity.

301 providing 32 individual trigger outputs and one OR32 trigger output. An Altera ARIA5  
 302 FPGA on the FEBv2 samples these trigger outputs at 400 MHz, recording rising and falling  
 303 times for the individual triggers and assigning time stamps to these. Time-over-threshold,  
 304 the difference between falling and rising times, gives some measure of signal amplitude.  
 305 This is used in addition to charge information and proves useful if there is more than  
 306 one hit per bar within the  $\sim 9 \mu\text{s}$  deadtime due to the readout of the multiplexed charge  
 307 output. The ARIA5 also manages the digitization of the sampled CITIROC multiplexed  
 308 HG and LG outputs via a 12-bit 8-ch ADC.

309 The internal 400 MHz clock on the FEBv2 can be synchronized to a common 100 MHz  
 310 clock. The synchronization subsystem combines input signals from the beam line into  
 311 a digital synchronization signal (SYNC) and produces a common detector clock (CLK)  
 312 which can eventually be synchronised to an external experiment clock. Both SYNC and  
 313 CLK signals are distributed to the FEBs. Tests show the FEB-to-FEB CLK(SYNC) delay  
 314 difference to be 50 ps (70 ps). Signals from the beam line at WAGASCI include two  
 315 separate timing signals, arriving 100 ms and 30  $\mu\text{s}$  before the neutrino beam at the near  
 316 detectors. The spill number is available as a 16-bit signal.

### 317 2.3.4 Pefromance check

318 All counters were measured at INR Moscow with a cosmic ray setup using the same type  
 319 S12571-025C MPPCs and a CAEN DT5742 digitizer. The average light yield (sum from  
 320 both ends) was measured to be 37.5 photo-electrons (p.e.) per minimum ionizing particle  
 321 (MIP) and 65 p.e./MIP for vertical and horizontal counters, respectively. After shipment  
 322 to CERN, all counters were individually re-tested with an LED [?]. 0.1% of counters  
 323 failed the LED tests and were therefore not used during the assembly of modules. The

324 assembly of modules was completed in June 2017, and it was then tested in June and July  
 325 2017 at the Proton Synchrotron experimental hall at CERN with a mixed particle beam  
 326 comprising mostly muons whose momenta could be selected between 0.5 and 5 GeV/c. An  
 event display from the summer 2017 tests is shown in Figure 14.

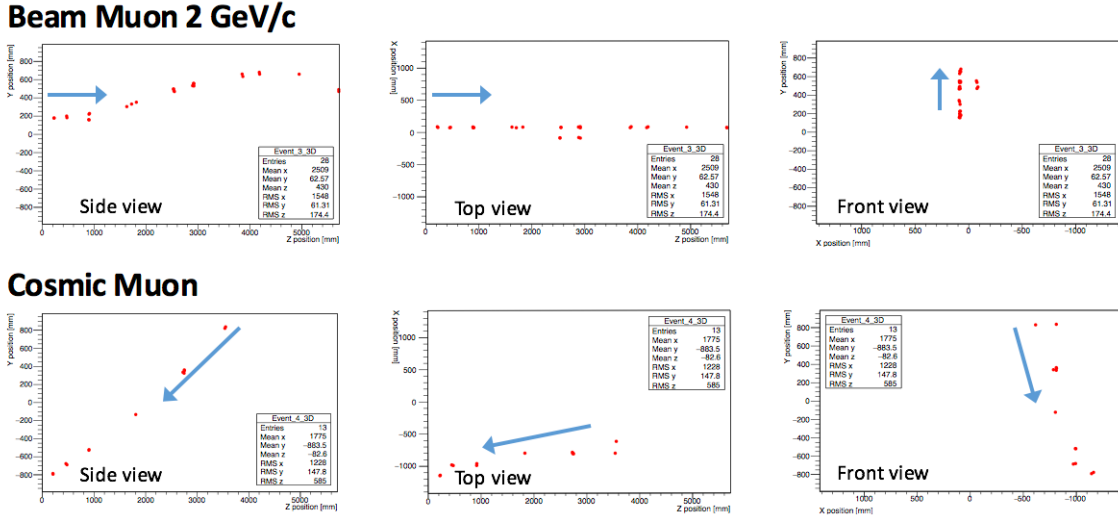


Figure 14: Comparison of a beam muon and cosmic muon in the three different geometrical projections of the detector. The beam impinges on the detector from the left. The arrows indicate the direction of travel of these muons. The direction of the cosmic muon is inferred from timing information.

327

## 328 2.4 Side muon range detector

329 Two Side-MRD modules for tracking secondary particles from neutrino interactions will be  
 330 installed in 2018. Each Side-MRD module is composed of 11 steel plates and 80 scintillator  
 331 slabs. The slabs are arranged as 10 layers installed in the 13 mm gaps between the 30 mm  
 332 thick plates. Each steel plate size is 30 mm × 1610 mm × 1800 mm. Total module size is  
 333 2236 mm×1630 mm×975 mm as shown in Figure 15 (left), weight is ∼8.5 tonne.

334 Scintillator bars were manufactured by Uniplast company in Vladimir, Russia. Polystyrene  
 335 based scintillators were extruded with thickness of 7 mm, then cut to the size of 7 × 200 ×  
 336 1800 mm<sup>3</sup>. Dopant composition is 1.5% PTP and 0.01% POPOP. Scintillator surface was  
 337 etched by a chemical agent to form a white diffuse layer with excellent reflective perfor-  
 338 mance. Ideal contact between the scintillator and the reflector raises the light yield up  
 339 to 50% comparing to an uncovered scintillator. A sinusoidal groove was milled along the  
 340 scintillator to provide uniform light collection over the whole scintillator surface. WLS Y11  
 341 Kuraray fiber of 1 mm diameter was glued with an optical cement EJ-500 in the S-shape

342 groove as shown in Figure 15(right). A minimum bending radius of 30 mm was used to  
 343 ensure the the Kuraray S-type fibers remained within specification. Both ends of the fiber  
 344 were glued into optical connectors which were themselves attached to the scintillator and  
 345 provide an interface to SiPMs, Hamamatsu MPPC S13081-050CS(X1).

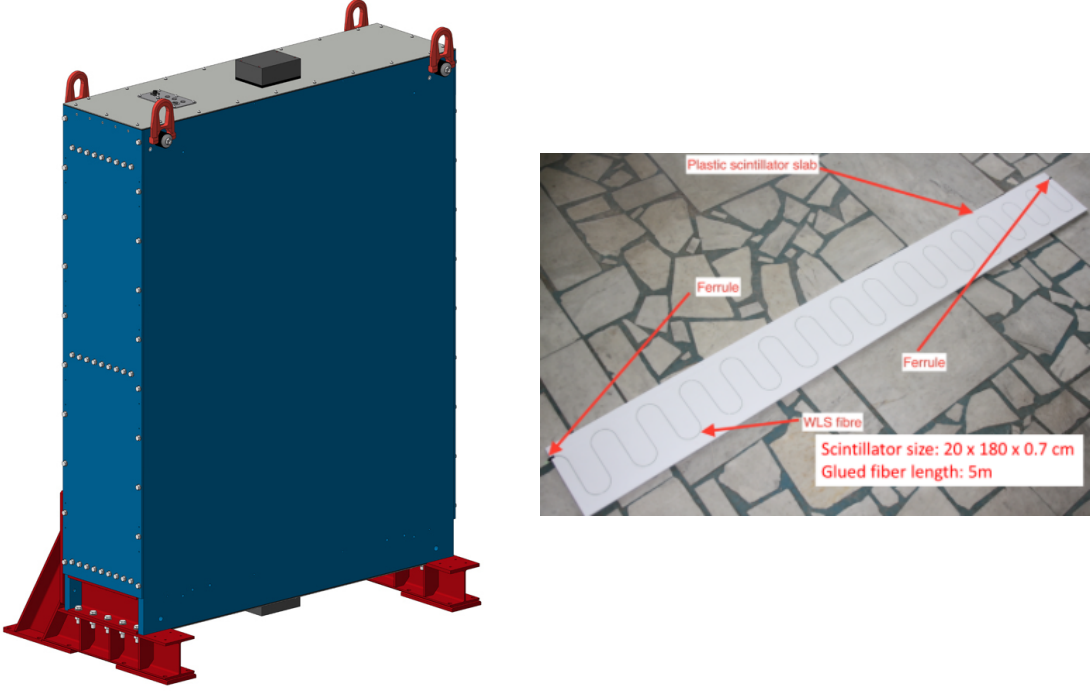


Figure 15: Left :Side-MRD module. Right: Scintillator bar of the Side-MRD modules.

346 Scintillators for the Side-MRD modules were assembled at INR in Russia, and shipped  
 347 to Japan in July 2017. The light yield for each scintillator was measured with cosmic  
 348 rays at INR and at YNU in Japan after delivery.  $LY_1$  and  $LY_2$  are light yields measured  
 349 at both ends of the counter. The light yield asymmetry between the ends calculated as  
 350  $100\% \times \frac{LY_1 - LY_2}{LY_1 + LY_2}$ . After tests at INR we selected 324 counters from measured 332 ones with  
 351 the mean light yield of 45 p.e./MIP (  $LY_1 + LY_2$  ) and the asymmetry value less than 10  
 352 % . The measuremens at YNU yielded the average total light yield of about 40 p.e./MIP  
 353 which varies in range from 32 to 50 p.e./MIP (Figure 16 (left)). Only two counters showed  
 354 relatively high asymmetry close to 25 % as shown in Figure 16 (right). Using the results of  
 355 the quality assurance test we selected 320 scintillator counters for the Side-MRD modules.

356 We also measured the time resolution for a combination of four counters piled one  
 357 upon another. The average result for four counters is  $\sigma_T = 1.04$  ns. The resolution of

358 combination of 2, 3, 4 counters is measured to be 0.79 ns, 0.66 ns and 0.58 ns, respectively.

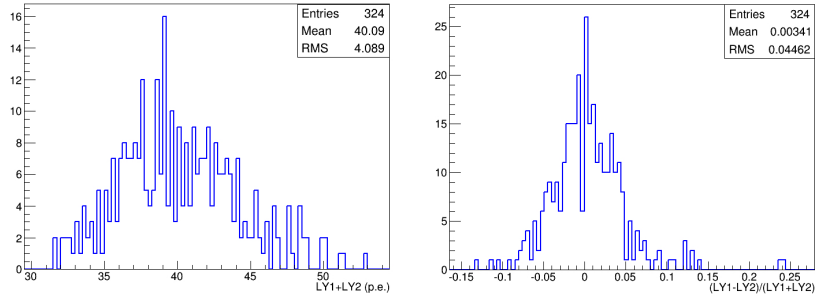


Figure 16: Total light yield distribution (left) and light yield assymetry (right) measured at YNU.

359  
360 Construction of the Side-MRD modules is scheduled from November 2017 at Yokohama  
361 National University. They will then be transported to J-PARC for installation on the B2  
362 floor of the T2K near detector hall.

363 Same electronics as the WAGASCI modules (see Sec. 2.1.2) are used for the Side-MRD  
364 modules.

### 365 3 Physics goals

366 We will measure the differential cross section for the charged-current (CC) interaction on  
367  $H_2O$  and Hydrocarbon(CH)). The water-scintillator mass ratio of the WAGASCI module  
368 is as high as 4:1 and the high purity measurement of the cross section on  $H_2O$  is possible.  
369 One experimental option is to remove water from one of the two WAGASCI modules. The  
370 water-out WAGASCI module will allow to measure pure-CH target interactions with very  
371 low momentum-threshold for protons. This will also allow this CH interaction background  
372 to be subtracted from the water-in target measurement. Another option is to add the T2K  
373 proton module which is fully made of plastic scintillators. It will allow the high statistics  
374 comparison of cross section between  $H_2O$  and CH and also comparison with the ND280  
375 measurement. The actual configuration will be optimized with detailed MC simulation by  
376 2018 Summer.

377 Our setup allows the measurements of inclusive and also exclusive channels such as  $1\mu$ ,  
378  $1\mu 1p$ ,  $1\mu 1\pi^\pm np$  samples, the first two of which are mainly caused by the quasi-elastic and  
379 2p2h interaction and the latter is mainly caused by resonant or coherent pion production  
380 and deep elastic scattering. In general, an accelerator produced neutrino beam spectrum is  
381 wide and the energy reconstruction depends upon the neutrino interaction model. There-

382 fore, recent neutrino cross section measurements including those from T2K are given as  
 383 a flux-integrated cross section rather than cross sections as a function of the neutrino en-  
 384 ergy to avoid the model dependency. We can provide the flux-integrated cross section.  
 385 In addition, by combining our measurements with those from ND280, model-independent  
 386 extraction of the cross section for narrow energy spread becomes possible. This method  
 387 was demonstrated in [1] and also proposed by E61 (NUPRISM) experiment.

### 388 3.1 Expected number of events

389 Expected number of CC neutrino events remaining after the event selections was evaluated  
 390 with simulation. Detailes are described in Sec. 5. In neutrino-mode, 5,400, 1,100 and 3,800  
 391 events are expected for the water-in WAGASCI module, the water-out WAGASCI module  
 392 and the INGRID proton module with  $5 \times 10^{20}$  POT. Among 5,400 events for the water-in  
 393 WAGASCI module, 78 % are interactions on H<sub>2</sub>O. In the antineutrino-mode, 2,240, 400  
 394 and 1,500 CC antineutrino events are expected for the water-in WAGASCI module, the  
 395 water-out WAGASCI module and the INGRID proton module with  $5 \times 10^{20}$  POT. Amongh  
 396 2,240, 74 % are interactions on H<sub>2</sub>O. The wrong-sign interactions in antineutrino-mode is  
 397 561 events, but will be removed with 90 % or higher efficiency by Baby MIND.

### 398 3.2 Pseudo-monochromatic beam by using different off-axis fluxes

399 The off-axis method gives narrower neutrino spectrum, and the peak energy is lower for  
 400 larger off-axis angle. There still remains a high energy tail mainly due to neutrinos from  
 401 Kaon decay. The off-axis angle of the WAGASCI location is 1.5 degrees as opposed to  
 402 2.5 degrees for ND280. Top two plots of Figure 17 show the energy spectra of fluxes and  
 403 neutrino interaction events at these two different location. Bottom two plots of Figure 17  
 404 show the energy spectra of fluxes and neutrino interaction events obtained by subtraction  
 405 of fluxes at ND280 and WAGASCI. We can effectively get two fluxes, from 0.2 GeV to  
 406 0.9 GeV and 0.6 GeV and 2 GeV and measure flux-integrated cross section for these two  
 407 fluxes. It should be noted that even though the statistical errors are drawn for each energy  
 408 bin for the bottom right plot of Fig. 17, measurement results will be given as an integration  
 409 across energies.

### 410 3.3 Extraction of Cross sections

The flux-integrated CC inclusive cross sections on H<sub>2</sub>O and CH are calculated from the  
 number of selected events with background subtraction and efficiency correction

$$\sigma_{CC} = \frac{N_{sel} - N_{BG}}{\phi T \epsilon},$$

411 where  $N_{sel}$  is the number of selected events from the real data,  $N_{BG}$  is the number of  
 412 contaminated background events,  $\phi$  is the integrated  $\nu_\mu$  flux,  $T$  is the number of target

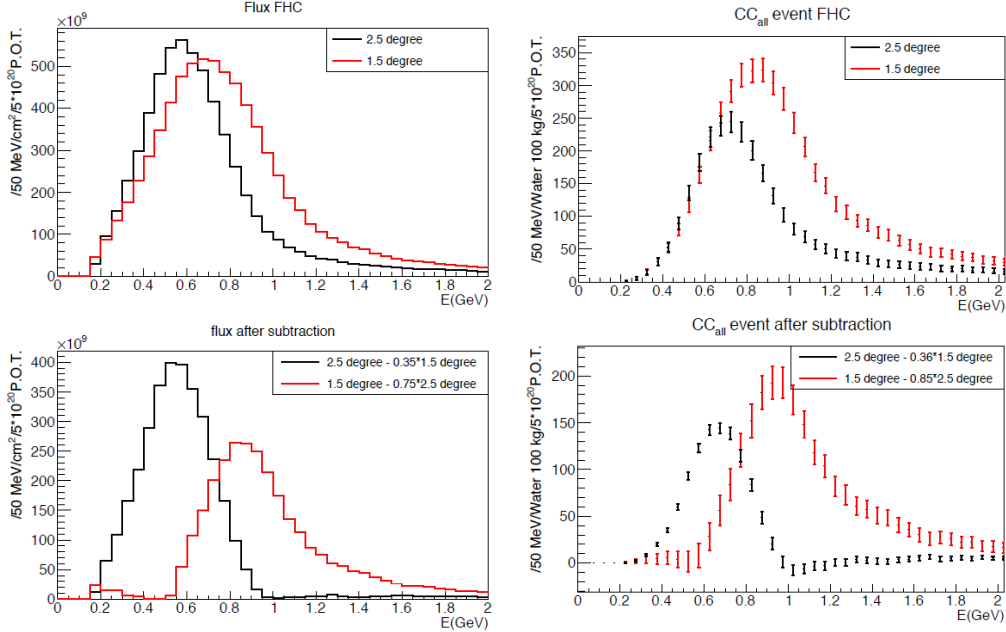


Figure 17: Energy spectra obtained by using different off-axis angle fluxes. Top two plots show the fluxes(left) and spectra of interaction events (right) for ND280 (off-axis 2.5 degree) and WAGASCI (off-axis 1.5 degree). Bottom two plots show the fluxes (left) and spectra of interaction events (right) obtained by subtraction of fluxes at ND280 and WAGASCI. The error bars represent the statistical error and those in the bottom right plot assume the statistical error for ND280 measurements are much smaller than those of the WAGASCI experiment.

413 nucleons, and  $\epsilon$  is the detection efficiency for signal estimated by MC simulation. The  
414 number of main background events is effectively estimated from side-band samples. The  
415 CH interaction background for the H<sub>2</sub>O measurement is estimated from the measurement  
416 of the Water-out WAGASCI module and/or the proton module. The neutrino interaction  
417 background for the antineutrino measurement is estimated from the opposite-sign inter-  
418 actions selected by Baby MIND. The dominant error for the inclusive total cross section  
419 measurement is the uncertainty of the neutrino flux, which is  $\sim 9\%$  now and is expected  
420 to be reduced to  $\sim 6\%$ . Since the flux error is dominated by the normalization type error,  
421 the flux error can be significantly reduced for the relative comparison of the H<sub>2</sub>O and CH  
422 cross sections and the relative comparison of the ND280 and WAGASCI measurements.  
423 For example, T2K INGRID succeeded to determine the cross section ratio for CH and  
424 Fe with 3% precision[5]. For the exclusive and/or differential cross section measurements,  
425 statistical error would be dominant, size of which depending on the binning.

#### 426 3.4 Subjects WAGASCI can contribute

427 Recent accelerator neutrino experiments use nuclear target e.g. organic scintillator, water  
428 and iron. So the interaction is largely affected by nuclear effects such as Fermi motion,  
429 correlated pairs of nucleons in nucleus (two particles-two holes, 2p2h), collective nuclear  
430 effects and final state interactions (FSI) of secondary particles in the nuclei after the initial  
431 neutrino interactions.

432 The main interaction type at the T2K energy (sub GeV) is the CC quasi-elastic (CCQE)  
433 interaction with nucleons inside nucleus. The energy is reconstructed from the lepton  
434 momentum assuming CCQE kinematics in T2K and other interactions would bias the  
435 reconstructed energy. Figure 18 shows how the reconstructed energy is affected. The 2p2h  
436 interactions mainly happen through the interaction with a correlated nucleons pair and also  
437 through the  $\Delta$  resonance interaction followed by pion-less decay. The 2p2h interactions  
438 are observed in electron scattering experiments [8] where the 2p2h events were observed  
439 in the gap between quasi-elastic region and pion-production region. Neutrino experiments  
440 have attempted to measure the 2p2h interactions, but so far there are only indicative  
441 results because the energy spectrum of the neutrino beam is wide and the precision of the  
442 event-by-event determination of the neutrino energy is not good nor suffered from bias. Our  
443 measurements, when combined with ND280 measurement, will give the cross section values  
444 for narrow energy-spread fluxes and give insight for such interactions. Another efficient  
445 way to investigate the 2p2h interaction is direct measurement of proton tracks with low  
446 momentum threshold and wide acceptance. Figure 19 left plot shows proton multiplicities  
447 for the CCQE events and 2p2h events. Figure 19 right plot shows opening angles of two  
448 proton-tracks for the events having two protons. The water-out WAGASCI can provide  
449 good sample for the 2p2h interaction search because its low density medium enables the  
450 detection of low momentum protons in side acceptance.

451 There are various models which describe the collective nuclear effects [9]. The wide

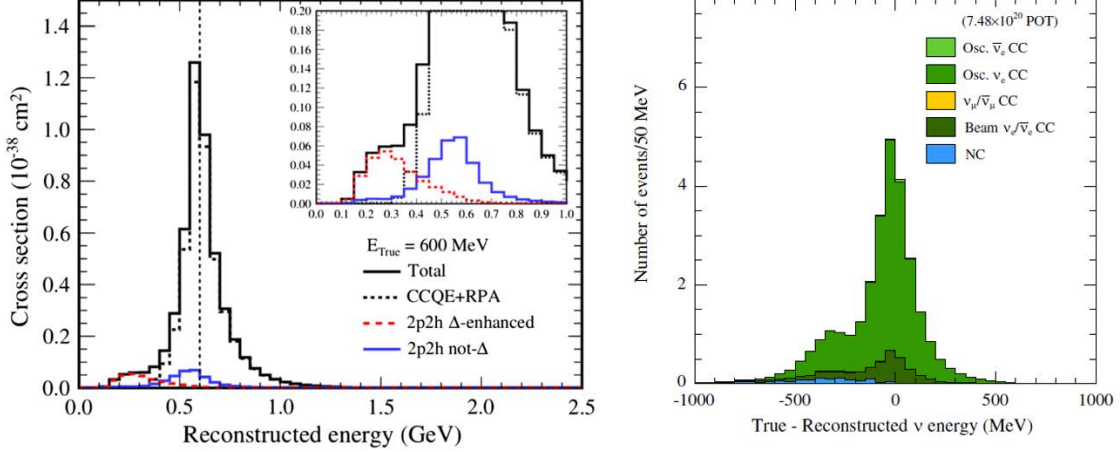


Figure 18: Left: reconstructed neutrino energy for CCQE and 2p2h interactions of 600 MeV muon neutrinos on  $^{12}C$  simulated with a mode. Right: difference between true and reconstructed energy of the  $\nu_e$  CCQE-like sample. The energy is reconstructed from the lepton momentum assuming the kinematics of the CCQE interaction. Both plots from [2]

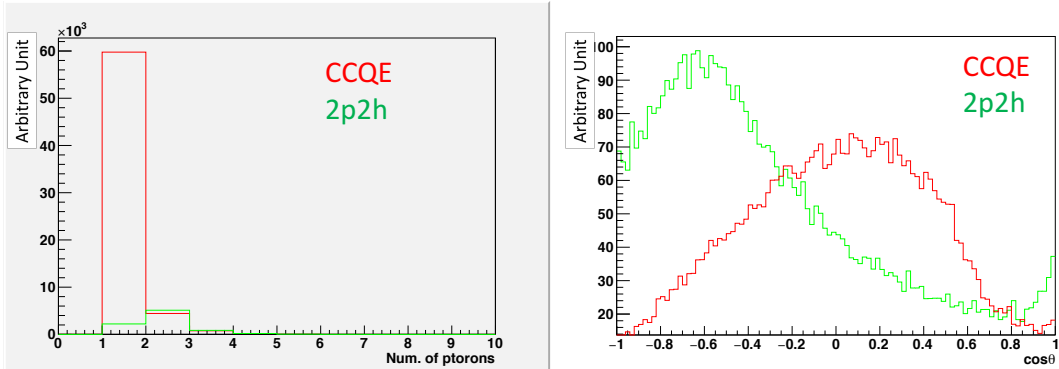


Figure 19: Proton multiplicities (left) and opening angles between two proton tracks (right) for CCQE events and 2p2h events. The final-state interaction is taking into account.

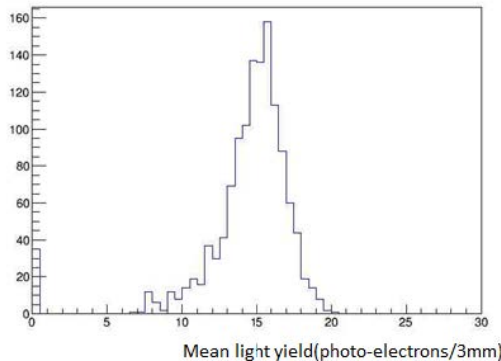
452 acceptance of the WAGASCI experiment will provide information complementary to ND280  
453 and will play important role to select and tune models.

454 T2K is starting to use  $\nu_e$  CC1 $\pi$  samples at the far detector to increase the statistics.  
455 One of the biggest uncertainty of the CC1 $\pi$  sample comes from the final state interac-  
456 tions of pions in the nuclei after the initial neutrino interactions because they change the  
457 multiplicity, charge and kinematics of the pions. The multi-pion production events can  
458 be migrated into the CC1 $\pi$  sample due to the FSIs, and they become backgrounds. The  
459 WAGASCI module has a capability to distinguish the pion track and proton track from  
460  $dE/dx$ , so WAGASCI can provide the CC1 $\pi$  cross section with low momentum threshold  
461 and wide acceptance for pion tracks.

## 462 4 Status of J-PARC T59 experiment

463 We had submitted a proposal of a test experiment to J-PARC in April 2014 to test a new  
464 detector with a water target, WAGASCI, at the neutrino monitor hall, and the proposal  
465 was approved as J-PARC T59. The project contains the side and downstream muon range  
466 detectors as well.

467 The first WAGASCI module has been constructed in 2016 and installed at the on-axis  
468 position in front of the T2K INGRID detector for the commissioning and the first cross  
469 section measurement as a part of the T2K experiment. The INGRID electronics boards are  
470 used to read the signal. The light yield measured with muons produced by the interaction  
471 of neutrinos in the hall wall, shown in Figure 20, is sufficiently high to get a good hit  
efficiency. A track search algorithm based on the cellular automaton has been developed



472 Figure 20: Light yield for muons produced by the interaction of neutrinos in the hall wall.  
473 Average light yields for each channel are plotted.

472 using the software tools from T2K INGRID. Examples of observed events are shown in  
473

474 Figure 21. The tracking efficiency in a 2-dimensional projected plane was evaluated by  
 475 comparing the reconstructed track in the WAGASCI module and the INGRID module,  
 476 and is shown in Figure 22. Note that that the tracking efficiency for high angle ( $> 70$  deg)  
 477 is not evaluated because of the acceptance of the INGRID module, not because of the  
 limitation of the WAGASCI module.

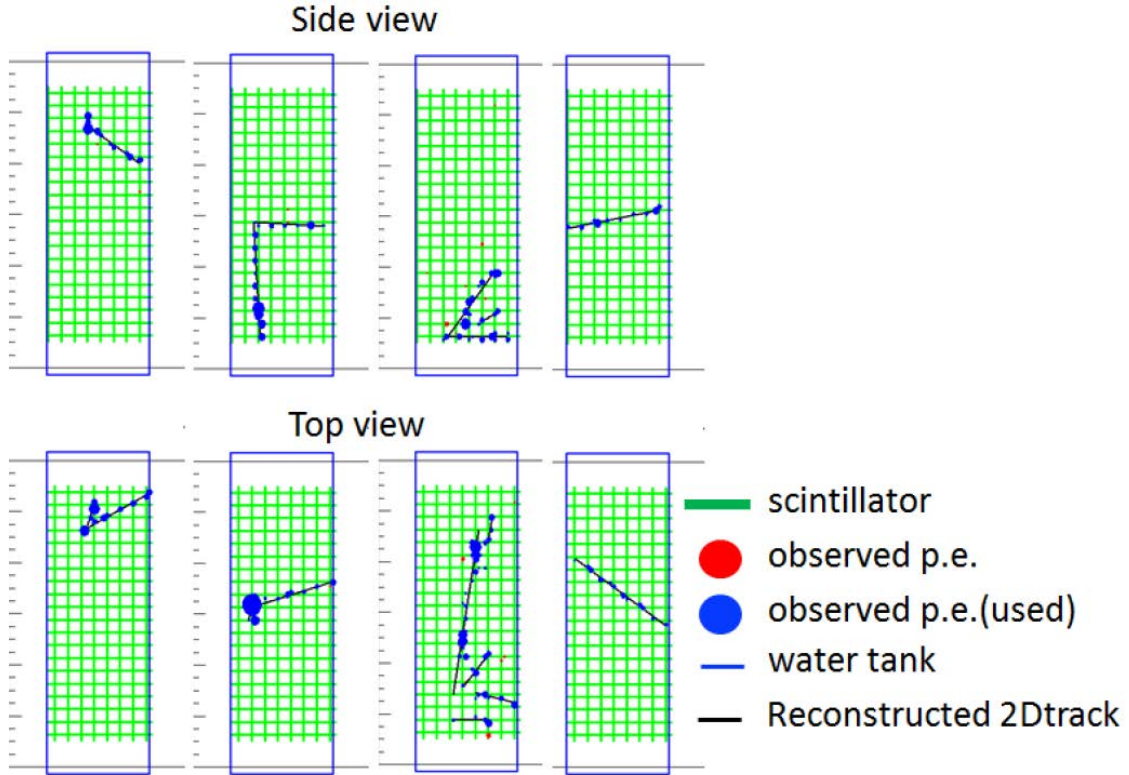


Figure 21: Example event displays of the WAGASCI module at on-axis. The reconstructed tracks are overlaid.

478  
 479 In 2017 Autumn, the construction of the second WAGASCI module and the dedicated  
 480 electronics board were completed. The module and the electronics were install on the B2  
 481 floor together with the T2K proton module and the INGRID module as shown in Figure 23.  
 482 The proton module is to be used as the entering muon veto and also for the comparison  
 483 of interaction between CH and Water. The INGRID module will act as the muon detector  
 484 for this period but due to its limited acceptance angle this is only a temporary measure.  
 485 The detector was commissioned and since October has been in operation taking data with  
 486 the T2K antineutrino beam.

487 The production of the components of the side muon range detectors has been completed

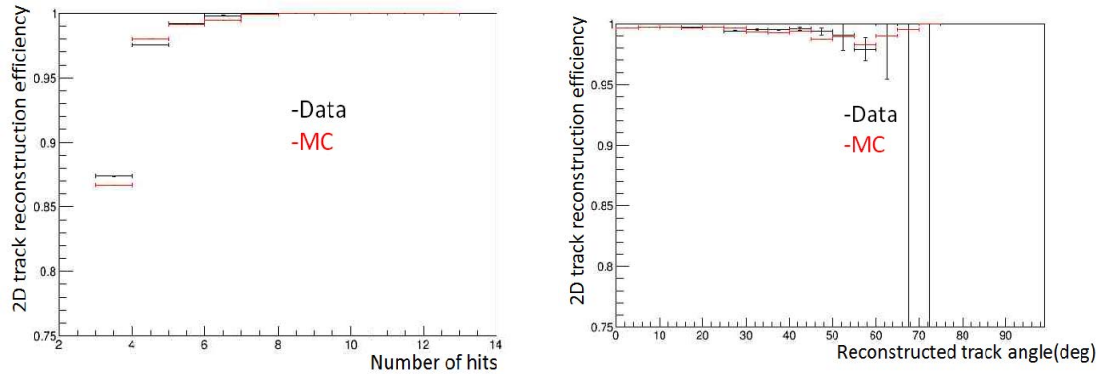


Figure 22: 2D track reconstruction efficiency as a function of number of hits (left) and track angle (right). Here the track angle is the one reconstructed by the INGRID module.

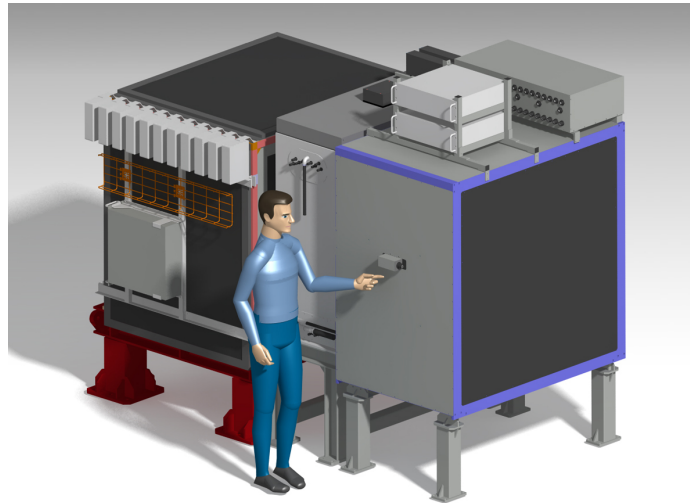


Figure 23: J-PARC T59 detector configuration in October 2017.

488 and now the detectors are being assembled at the Yokohama National University. These  
489 detectors will be installed between January and June 2018, when T2K is not running.

490 The Baby MIND detector was transported from CERN to Japan in December, 2017.  
491 It will be installed and commissioned in Jan.-Feb. 2018 and T59 will take the neutrino-  
492 induced muon data in April and May.

## 493 5 MC studies

### 494 5.1 Simulation setup

495 The expected number of neutrino events in the water-in Wagasci detector is predicted by  
496 Monte Carlo simulations. Neutrino beam flux at the detector location is simulated by  
497 T2K neutrino flux generator, JNUBEAM. Neutrino interactions with target materials are  
498 simulated by a neutrino interaction simulator, NEUT. Detector responses are simulated  
499 using GEANT4-based simulation.

500 The detector geometry in the simulation so far is different from the actual setup as  
501 shown in Figure 24. The active neutrino target region consists of four WAGASCI modules.  
502 The size of the WAGASCI module is same as the actual one: 1000 mm × 1000 mm in the  
503 x and y directions and 500 mm along the beam direction (z-direction). Two Side-MRD  
504 modules are installed either side of the Wagasci modules. Each Side-MRD module consists  
505 of ten iron plates whose dimension is 30 mm (thickness) × 2000 mm (height) × 3200 mm  
506 (width). The distance between the Side-MRD modules and WAGASCI modules is 800  
507 mm. The downstream-MRD is equivalent to the Baby-MIND, but without the magnetic  
508 field. It consists of thirty iron plates whose dimension is 30 mm (thickness) × 2000 mm  
509 (height) × 4000 mm (width). The distance between the downstream-MRD modules and  
510 WAGASCI modules is 800 mm. Update of the study with the actual geometry is now  
511 underway.

512 To simulate the signal, the energy deposit inside the scintillator is converted into the  
513 number of photons. The effects of collection and attenuation of the light in the scintillator  
514 and the WLS fiber are simulated, and the MPPC response is also taken into account. The  
515 light yield is smeared according to statistical fluctuations and electrical noise.

### 516 5.2 Event selection

517 Tracks are reconstructed in two-dimensional planes in each sub-detector. Then, track  
518 matching among the sub-detectors and three-dimensional track reconstruction are per-  
519 formed. These analysis tools have been developed from the software tools by the T2K  
520 INGRID and in mature stage already.

521 The events are selected as follows. The starting point of the track is required to be  
522 50 mm away from the edge of the WAGASCI module. This is to remove the background  
523 from the outside. The longest track has to penetrate more than one (five) iron plates in

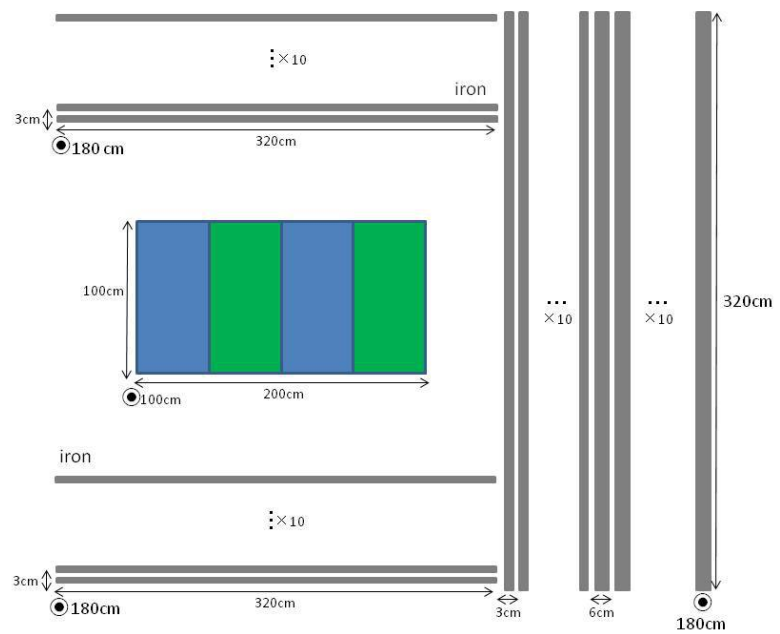


Figure 24: Geometry of the detectors in the Monte Carlo simulation.

524 Side-MRD modules (Baby-MIND). This cut select a muon track and rejects backgrounds  
 525 from NC and neutral particles. Then, in order to determine the muon momentum, it is  
 526 required that the longest track stops in MRDs (Side-MRD modules and Baby-MIND) or  
 527 penetrate all iron plates.

528 Table 1 shows numbers of the selected events in one water-in WAGASCI module after  
 529 the event selection. We expect 4,239 (1,666) events from charged-current interaction on  
 530 H<sub>2</sub>O with  $5 \times 10^{20}$  POT in (anti)neutrino-mode with one water-in WAGASCI module.  
 531 The purity, when interactions on CH is counted as background, is 78% for the neutrino-  
 532 mode. There is a significant contamination from the wrong-sign (neutrino) interaction for  
 533 antineutrino-mode, however, we expect that it will be removed with efficiency higher than  
 90% by Baby MIND.

Table 1: Expected number of the selected neutrino-candidate events in one water-in WA-GASCI module with  $5 \times 10^{20}$  POT in each of neutrino-mode and antineutrino-mode. Note that the wrong sign component will be reduced by one order by applying the charge selection by Baby MIND.

|                   | CC on H <sub>2</sub> O | NC on H <sub>2</sub> O | Interaction on CH | wrong sign interaction |
|-------------------|------------------------|------------------------|-------------------|------------------------|
| $\nu$ -mode       | 4239                   | 107                    | 1087              | (negligible)           |
| anti- $\nu$ -mode | 1666                   | 14                     | 560               | (561)                  |

534  
 535 Table 2 and 3 summarize contributions classified by the interaction types and final state  
 topologies for the selected charged current-interaction events, respectively.

Table 2: Interaction types for the selected charged-current events.

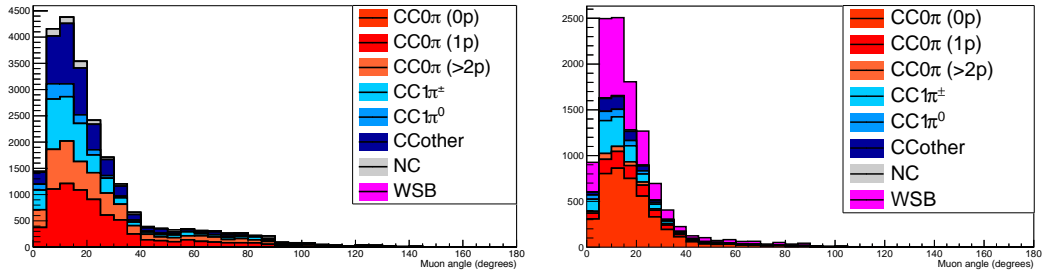
|                   | CCQE   | 2p2h  | CC resonant $\pi$ | CC-DIS |
|-------------------|--------|-------|-------------------|--------|
| $\nu$ -mode       | 48.4 % | 9.7 % | 27.1 %            | 14.7 % |
| anti- $\nu$ -mode | 57.1 % | 8.2 % | 17.3 %            | 17.3 % |

Table 3: Final state topologies for the selected charged-current events.

|                   | CC0 $\pi$ | CC1 $\pi$ | CC2 $\pi$ | CCn $\pi$ |
|-------------------|-----------|-----------|-----------|-----------|
| $\nu$ -mode       | 67.4 %    | 20.9 %    | 3.0 %     | 8.7 %     |
| anti- $\nu$ -mode | 79.5 %    | 16.3 %    | 1.2 %     | 3.0 %     |

536  
 537 Figure 25 shows the reconstructed angles of the longest tracks in the selected events in  
 538 the neutrino-mode and the anti-neutrino mode. Figure ?? shows the iron plane numbers

539 in Side-MRD and Baby-MIND corresponding to the end points of the longest tracks in the  
selected events in the neutrino-mode and the anti-neutrino mode.



540 Figure 25: The reconstructed angles of the longest tracks in the selected events in the  
neutrino-mode (left) and the antineutrino-mode (right).

## 541 6 Standalone WAGASCI-module performances

542 In the previous sections, the WAGASCI detector was studied using the Muon Range Detectors.  
543 In this section, the standalone abilities of WAGASCI module are presented. Using  
544 the WAGASCI configuration presented in Section 5, we have evaluated that only 7% of  
545 the muons will be stopped in one of the WAGASCI modules. However, this proportion  
546 increases to 53% for pions and 73% for protons produced by neutrino interactions at  $1.5^\circ$   
547 off-axis. Figure 27 shows the momentum distribution of these daughter particles as well as  
548 for the sub-sample stopped in one of the WAGASCI modules. Therefore, the study of the  
549 standalone abilities of the WAGASCI module in this section are dominantly motivated by:

- 550 • the accurate measurement of the neutrino interaction final states. Though most of  
551 the muons will be reconstructed and identified in the MRDs, the hadronic particles  
552 will predominantly stop in one of the WAGASCI modules. One has therefore to rely  
553 exclusively on the WAGASCI module information alone to reconstruct, identify and  
554 measure the momentum of pions or protons.
- 555 • the coverage of the MRDs is not  $4\pi$ . Using the WAGASCI module information can  
556 therefore help to constrain the particles that exit the WAGASCI module but do not  
557 enter any MRD.
- 558 • the particle identification of low momenta muons  $p_\mu < 300$  MeV/c that will leave  
559 only a few hits in the MRD. Using the WAGASCI module information will clearly  
560 enhance the particle identification.

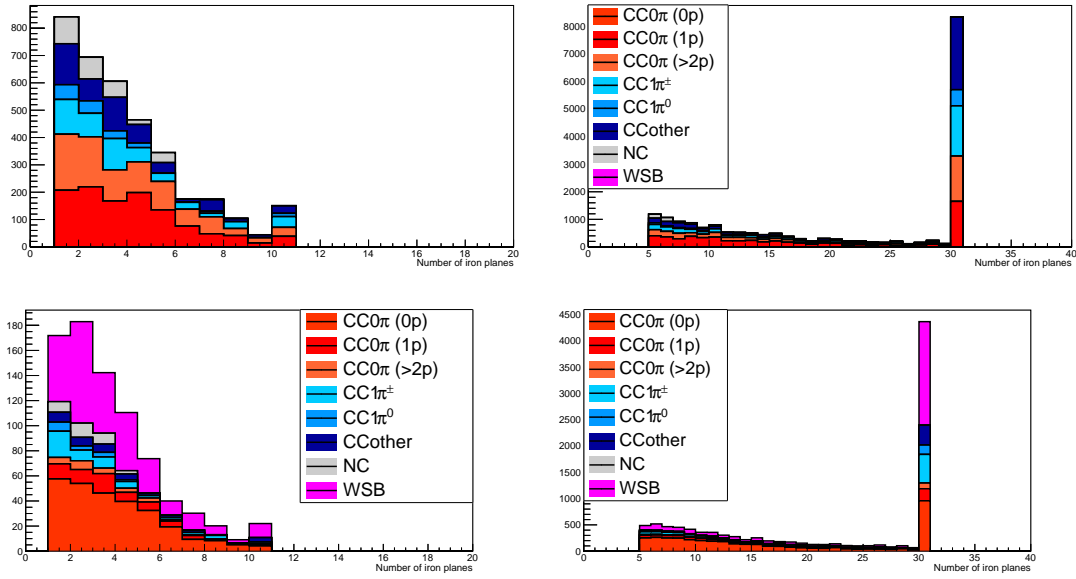


Figure 26: Iron plane numbers in Side-MRD (left) and Baby-MIND (right) corresponding to the end points of the longest tracks in the selected events in the neutrino-mode (top) and the antineutrino-mode (bottom).

561 This study is based on an original study done for the ND280 upgrade target, with some  
 562 modifications. Though the cell size is similar to the WAGASCI configuration presented  
 563 in Section 5, the external dimensions are different (1864 mm  $\times$  600 mm  $\times$  1300 mm).  
 564 Whenever the results are presented with this external size and this parameter is likely to  
 565 impact the result, it will be mentioned.

566 Note that in this section, a simplified reconstruction algorithm presented in Section 6.1 is  
 567 used. The fiducial volume is chosen accordingly as the inner cube of the module which  
 568 surfaces are  $4 \times$  scintillator space = 100 mm distant from the module external surfaces.  
 569 The neutrino interactions are simulated using NEUT v5.3.2. The NEUT input neutrino  
 570 flux is estimated using JnuBeam v13a and assuming the detector to be located at  $1.5^\circ$   
 571 off-axis, as in Section 5. Note that the event reconstruction efficiency as a function of true  
 572 neutrino energy might be changed at  $1.5^\circ$ , due for example to different  $Q^2$  distributions.  
 573 For this reason, one has to note that the reconstruction results might change slightly from  
 574  $2.5^\circ$  and  $1.5^\circ$ . To avoid a similar change on the particle-only reconstruction efficiencies,  
 575 they will be presented as a function of variables that completely characterize the particle  
 576 kinematic state, *i.e.* its momentum and angle. Figure 28 shows the vertex distributions  
 577 of the daughter particles of neutrinos interacting one standard WAGASCI water-module.  
 578 In this section, we will show the detector reconstruction and particle identification in this

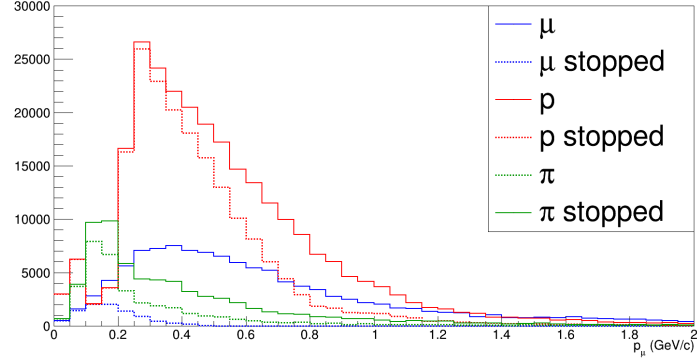


Figure 27: Momentum distribution of true particles in WAGASCI (plain) and corresponding distributions only for particles stopping into the WAGASCI module (dashed).

phase space, both for leptonic and hadronic particles. We will finally show an empty WAGASCI module can highly enhance the ability to constrain the neutrino interaction final state which is critical to reduce the corresponding uncertainties.

## 6.1 Reconstruction algorithm

### 6.1.1 Description

For this section, an ideal “simulated” reconstruction is developed. A particle is reconstructed if:

1. The particle is charged.
2. Has at least one hit (energy deposit  $> 2.5$  photo-electron) in a scintillator.
3. The particle enters one TCP and has one hit in the tracker.

Or

591

- 592 • The particle should be long enough to be reconstructed by the detector in at  
593 least 2 out of 3 views (XZ, YZ, XY). The length criterion requires the particle  
594 to let at least 4 hits in the detector. In the “less favourable case” of pure  
595 longitudinal or transverse going tracks, it represents a the track length of  $L_{track} \geq$   
596  $4 \times$  scintillator space = 100 mm.
- 597 • In the views where particles pass the length criterion, the particle shall not  
598 be superimposed with longer tracks in at least two views. The superposition  
599 criterion is estimated with the distance inter-tracks (DIT) which corresponds to

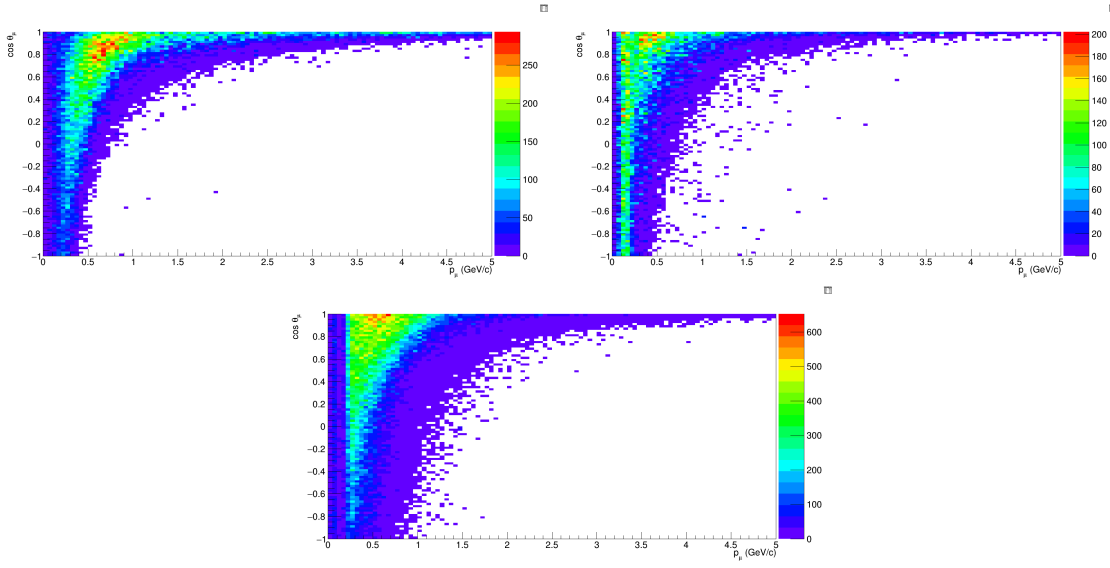


Figure 28: True number of muons (left), charged pions (right) and protons (bottom) in the two WAGASCI water-module as a function of the particles momenta and angles at  $1.5^\circ$ .

the orthogonal distance between two tracks at the ending point of the shortest one (see Figure 29). For a track we call track 1, the super position criterion is tested with every longer track that starts at the same vertex. Let  $\vec{p}_1$  the vector of track 1, and  $p_1^a$  its projections in the XZ, YZ and XY planes respectively for  $i=1,2,3$ . Note that these are projections onto 2D planes and not onto a direction vector. In this case, the relative angle between track 1 and a longer track, track 2, (of vector  $\vec{p}_2$ ) in a view a is given by:

$$\cos \theta = \frac{\vec{p}_1^a \cdot \vec{p}_2^a}{\|\vec{p}_1^a\| \|\vec{p}_2^a\|} \quad (1)$$

and the distance inter track is given by:

$$DIT = \|\vec{p}_1^a\| \sin \theta \quad (2)$$

The DIT should be higher than  $4 \times$  scintillator width for the track 1 to be not superimposed with the track 2 in the view a, which also corresponds to 100 mm in the nominal configuration.

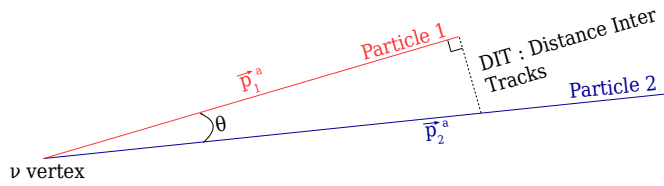


Figure 29: Definition of the distance inter tracks.

### 6.1.2 Performances

The particle-only reconstruction efficiencies and the reconstruction threshold in momenta are shown in Table 4. This threshold is defined as the maximal momentum for which the reconstruction efficiency is smaller than 30%. The thresholds in muon and pion momenta are 150 MeV/c. Most of the muons are above this threshold (see Figure 28) which leads to a 79% reconstruction efficiency.

|                           | $\mu$     | $\pi$     | p         |
|---------------------------|-----------|-----------|-----------|
| Reconstruction Efficiency | 79%       | 52%       | 26%       |
| Momentum threshold        | 150 MeV/c | 150 MeV/c | 550 MeV/c |

Table 4: Reconstruction efficiency and momentum threshold for muons, pions and protons. The threshold is defined as the maximal momentum for which particles have a reconstruction efficiency smaller than 30%.

The lower pion and proton efficiencies (respectively 52% and 26%) are due to lower efficiencies for similar momenta than muons, coming from strong interactions as shown on Figures 30. Efficiencies of each particle type tend to decrease in the backward region due to lower particle momenta. However, for a fixed momentum value, the reconstruction efficiency is almost uniform which confirms the ability of the WAGASCI detector to reconstruct high angle tracks.

The reconstruction is thereafter tested on neutrino events. Table 5 summarizes the number of reconstructed events and efficiencies for each interaction type. As expected from the high muon reconstruction efficiency, the charged current interactions have reconstruction efficiencies  $\geq 85\%$ .

The reconstruction efficiencies as a function of the neutrino energy and muon kinematics are respectively shown on Figure 31 and 32.

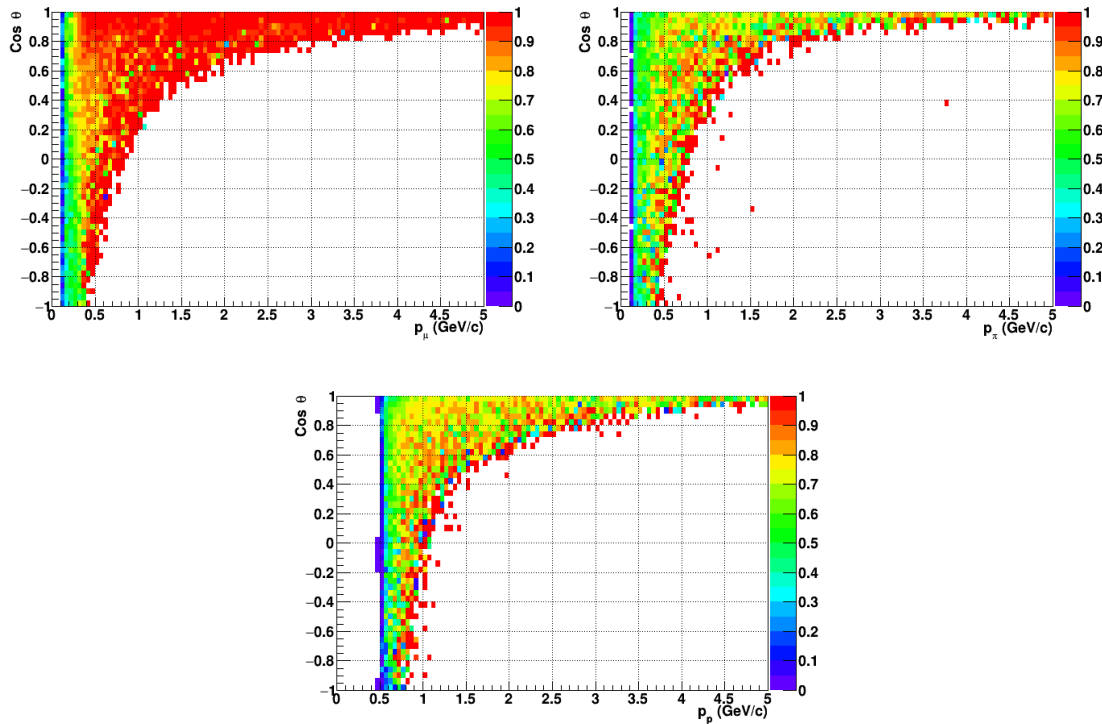


Figure 30: Reconstruction efficiency of muons (left), charged pions (right) and protons (bottom) in the WAGASCI water-module as a function of the particles momenta and angles.

|                           | CC0 $\pi$ | CC1 $\pi$ | CCOthers | NC  | All |
|---------------------------|-----------|-----------|----------|-----|-----|
| Reconstruction efficiency | 85%       | 87%       | 91%      | 22% | 68% |

Table 5: Number of true interactions reconstructed. The purity and reconstruction efficiency of each true interaction is also shown.

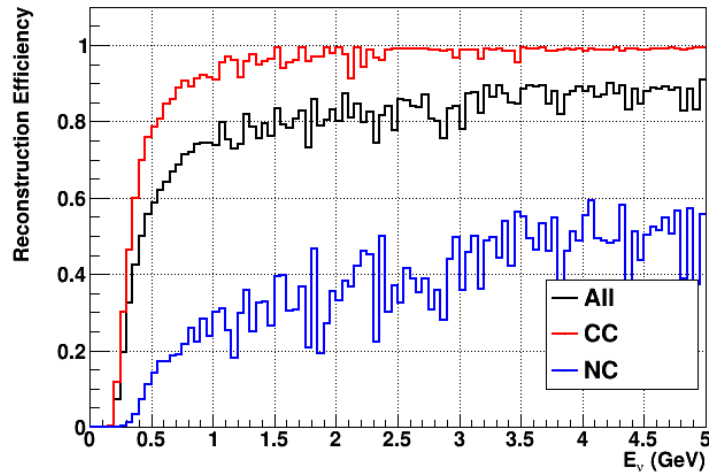


Figure 31: Reconstruction efficiency of all neutrino (black), CC (red) and NC (blue) interactions in the WAGASCI water-module as a function of the neutrino energy.

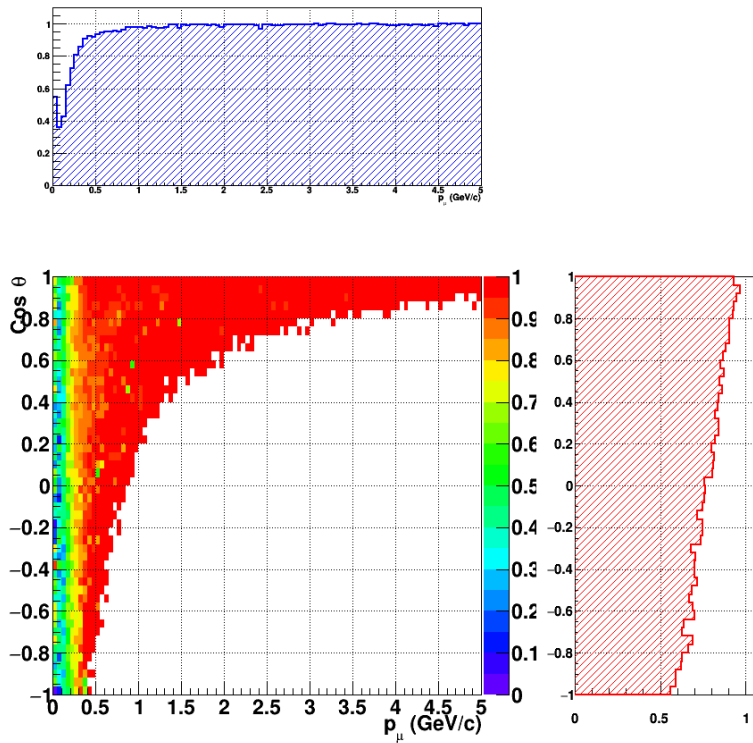


Figure 32: Reconstruction efficiency of CC interactions in the WAGASCI water-module as a function of the muon kinematic variables (momentum and angle).

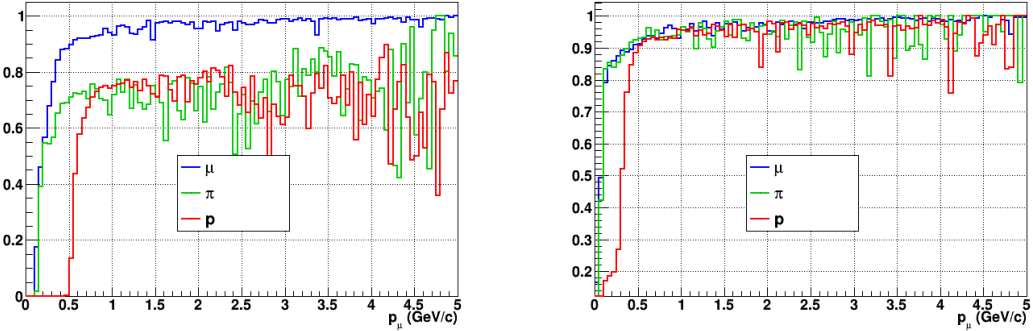


Figure 33: Reconstruction efficiency for muons, pions and protons in the water-in (left) and water-out (right) modules.

629 Note that a Particle Identification Algorithm has been also developed. It is based on  
 630 the charge deposition of the particles in the scintillator, of the detection of a decay-electron.  
 631 However, information depends highly on the number of scintillator hits by a particle, which  
 632 creates an important difference between a real WAGASCI module and the one used for the  
 633 ND280-upgrade simulation. For this reason, the corresponding results will not be detailed  
 634 here, but can be found in [?].

## 635 6.2 Background subtraction: the water-out module

636 In the nominal configuration, 20% of the neutrino interactions occurs on scintillators  
 637 ( $C_8H_8$ ). This background should be removed in order to measure the neutrino interac-  
 638 tion on the same target as Super-K, which suppress the differences in cross-section models.  
 639 For this purpose, we propose to use a water-out module, where the water is replaced by  
 640 air. The detector is therefore fully active and has a 3 mm spatial resolution (scintillator  
 641 thickness) which create an ideal detector to reconstruct and identify hadrons, and study  
 642 np-nh interactions. The counter-part is the difference in particle energy deposition between  
 643 the water and this water-out module that will need to be corrected for. In this section,  
 644 we present the capabilities of such a module, and the impact it can have on cross-section  
 645 measurements for the neutrino community in general and T2K in particular.  
 646 The same reconstruction and selection as the water-in module is applied. Figure 33 shows  
 647 the comparison between the water-in and the water-out reconstruction efficiencies for muon,  
 648 pions and protons. 90% of the muons and 87% of the pions are reconstructed, while 70%  
 649 of the protons are even reconstructed. It allows to lower down the proton threshold to  
 650 250 MeV/c (see Table 6).

651 As a consequence of tracking even low momenta particle, the reconstruction efficiency  
 652 is uniform and almost maximal on the entire  $\cos \theta_\mu$  phase space, as shown on Figure 34.

|   | $\mu$           | $\pi$           | p                |
|---|-----------------|-----------------|------------------|
| Reconstruction Efficiency<br>Momentum threshold | 90%<br>50 MeV/c | 87%<br>50 MeV/c | 70%<br>250 MeV/c |

Table 6: Reconstruction efficiency, proportions of  $\mu$ -like and non  $\mu$ -like and momentum threshold for muons, pions and protons in the empty module. The threshold is defined as the maximal momentum for which particles have a reconstruction efficiency smaller than 20%.

653 Since the fiducial mass represents 0.25 tons, the total number of events is divided by a  
 654 factor of 3 compared to the water-in module. The water-out module offers interesting  
 655 possibilities to study np-nh interaction since 70% of the protons are reconstructed. In the  
 656 future, a possible separation as a function of the number of proton track will be studied.  
 657 Moreover, we are currently pursuing the use of single and double transverse variables (cite  
 658 Xianguo) to open new possibilities for separating np-nh from Final State Interactions, or  
 659 for isolating the interactions on hydrogen from interactions on carbon in this module.

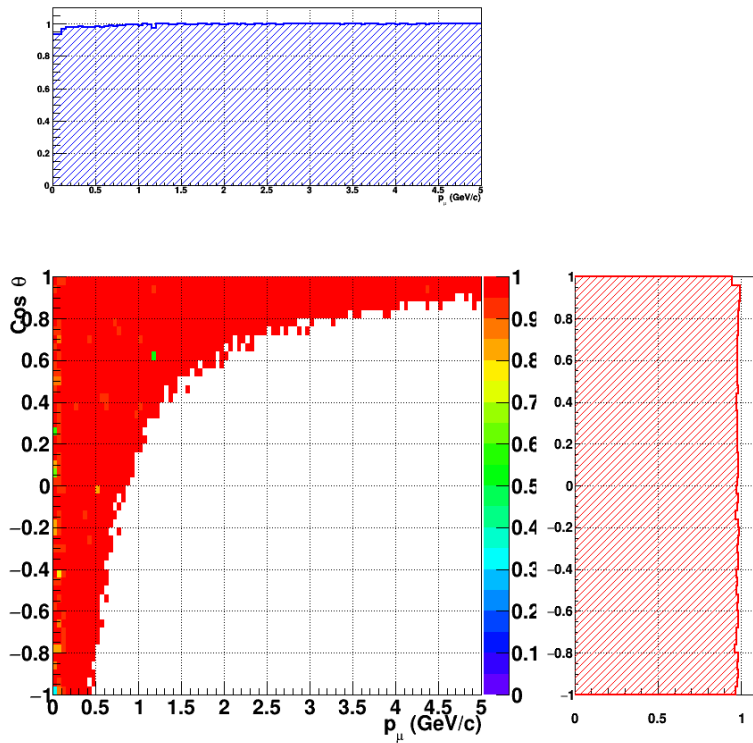


Figure 34: Reconstruction efficiency of CC interactions in the WAGASCI empty module as a function of the muon kinematic variables (momentum and angle).

660 **7 Schedule**

661 We would like to start a physics data taking from T2K beam time after the summer  
662 shutdown in 2018. By then, commissioning and tests of the detectors will be completed  
663 in J-PARC T59. The experiment can run parasitically with T2K, therefore we request no  
664 dedicated beam time nor beam condition as discussed in the following section.

665 Once the approved POT is accumulated, the WAGASCI modules will be removed  
666 from the experimental site, but we would like to keep the Baby-MIND and the Side-MRD  
667 modules on the B2 floor of the NM pit as common platforms of future neutrino experiments  
668 using the T2K neutrino beam.

669 **8 Requests**

670 **8.1 Neutrino beam**

671 The experiment can run parasitically with T2K, therefore we request no dedicated beam  
672 time nor beam condition. As data taking periods, we request the ‘nominal’ T2K one-year  
673 operation both for the neutrino beam and the antineutrino beam. The T2K has been  
674 requesting  $0.9 \times 10^{21}$  POT/year and actually accumulating about  $0.7 \times 10^{21}$  POT/year in  
675 recent years. For each year, starting from the Autumn, T2K is running predominantly in  
676 the neutrino mode or in the antineutrino mode. Our request is to have one-year neutrino-  
677 mode data and another one-year antineutrino mode data assuming that the POT for the  
678 fast extraction in each year is more than  $0.5 \times 10^{21}$  POT.

679 **8.2 Equipment request including power line**

680 We request the followings in terms of equipment on the B2 floor:

- 681 • Site for the WAGASCI modules, Side-MRD modules and BabyMIND and their elec-  
682 tronics system on the B2 floor of the near detector hall (Figure 2 and 3).
- 683 • Anchor points (holes) on the B2 floor to secure the WAGASCI modules, Side-MRD  
684 module and Baby-MIND, detailed floor plans to be communicated in a separate  
685 document.
- 686 • Power line for the magnets in Baby-MIND: 400 V tri-phase 48-to-62 Hz, capable of  
687 delivering 12 kW. We have a wish for the magnet power line to be installed and  
688 available to us by beginning of March 2018.
- 689 • Electricity for electronics and water circulation system, 3 kW, standard Japanese  
690 electrical sockets.

- 691 1. Online PCs: 2.1 kW

692            2. Electronics: 0.7 kW

693            3. Water sensors: 1 kW

- 694        • Air conditioner for cooling heat generation at Baby-MIND magnets, online PCs and  
695            electeronics
- 696        • Beam timing signal and spill information
- 697        • Network connection

698        The infrastructure for much of the above exists already. Exceptions are the power line  
699        for the magnet and the electronics and holes in the B2 floor to anchor the detector support  
700        structures.

## 701        References

- 702        [1] K. Abe et al. Measurement of the muon neutrino inclusive charged-current cross  
703            section in the energy range of 13 GeV with the T2K INGRID detector. *Phys. Rev.*,  
704            D93(7):072002, 2016.
- 705        [2] K. Abe et al. Measurement of neutrino and antineutrino oscillations by the T2K  
706            experiment including a new additional sample of  $\nu_e$  interactions at the far detector.  
707            *Phys. Rev.*, D96(9):092006, 2017.
- 708        [3] M. Antonova et al. Baby MIND Experiment Construction Status. In *Prospects in*  
709            *Neutrino Physics (NuPhys2016) London, London, United Kingdom, December 12-14,*  
710            2016, 2017.
- 711        [4] K. Nitta et al. The k2k scibar detector. *Nucl. Instrum. Meth. A*, 535:147, 2004.
- 712        [5] K. Abe et al. (T2K Collaboration). Measurement of the inclusive  $\nu_\mu$  charged current  
713            cross section on iron and hydrocarbon in the t2k on-axis neutrino beam. *Phys. Rev.*  
714            D, 90:052010, 2014.
- 715        [6] F. Magniette F. Gastaldi, R. Cornat and V. Boudry. A scalable gigabit data acquisition  
716            system for calorimeters for linear collider. *proceedings of TIPP2014*, page PoS 193,  
717            2014.
- 718        [7] J. Fleury, S. Callier, C. de La Taille, N. Seguin, D. Thienpont, F. Dulucq, S. Ahmad,  
719            and G. Martin. Petiroc and Citiroc: front-end ASICs for SiPM read-out and ToF  
720            applications. *JINST*, 9:C01049, 2014.
- 721        [8] M. B. Barbaro J. A. Caballero T. W. Donnelly G. D. Megias, J. E. Amaro. Inclusive  
722            electron scattering within the susav2 meson-exchange current approach. *Phys. Rev.*  
723            D, 94:013012, 2016.

- 724 [9] M. Valverde J. Nieves, J. E. Amaro. Inclusive quasi-elastic neutrino reactions. *Phys.*  
725 *Rev. C*, 70:055503, 2004.
- 726 [10] Yu. G. Kudenko, L. S. Littenberg, V. A. Mayatsky, O. V. Mineev, and N. V. Ershov.  
727 Extruded plastic counters with WLS fiber readout. *Nucl. Instrum. Meth.*, A469:340–  
728 346, 2001.
- 729 [11] O. Mineev, Yu. Kudenko, Yu. Musienko, I. Polyansky, and N. Yershov. Scintillator  
730 detectors with long WLS fibers and multi-pixel photodiodes. *JINST*, 6:P12004, 2011.
- 731 [12] Etam Noah et al. Readout scheme for the Baby-MIND detector. *PoS*, Photo-  
732 Det2015:031, 2016.
- 733 [13] Omega. Spiroc 2 user guide. 2009.